Geol. Mag. **152** (*6*), *2015, pp. 1085–1103. © Cambridge University Press 2015*
doi:10.1017/S0016756815000187

Questioning a widespread euxinia for the Furongian (Late Cambrian) SPICE event: indications from $\delta^{13}C$, $\delta^{18}O$, $\delta^{34}S$ and biostratigraphic constraints

THOMAS WOTTE*† & HARALD STRAUSS‡

*Institut für Geologie und Mineralogie, Universität zu Köln, Zülpicher Strasse 49a, D-50674 Köln, Germany
‡Institut für Geologie und Paläontologie, Westfälische Wilhelms-Universität Münster, Corrensstrasse 24, D-48149 Münster, Germany

(*Received* 12 December 2014; *accepted* 17 March 2015; *first published online* 20 May 2015)

Abstract – Results from a high-resolution study of $\delta^{13}C_{carb}$, $\delta^{18}O_{carb}$, $\delta^{34}S_{CAS}$, $\delta^{34}S_{CRS}$ and elemental concentrations (Ca, Fe, Mg, Mn and Sr) in the Furongian Kyrshabakty section, southern Kazakhstan, are reported here. The investigated interval covers the Drumian to Jiangshanian stages of the Cambrian Period, respectively the regional *Ptychagnostus atavus* to *Ivshinagnostus ivshini-Irvingella major* trilobite zones. $\delta^{13}C_{carb}$ data include the Steptoean positive carbon isotope excursion (SPICE) with a local peak value of +5 ‰. The onset of SPICE corresponds to the *Kormagnostus simplex – Glyptagnostus stolidotus* zones and pre-dates the base of the Paibian Stage/Furongian Series. $\delta^{34}S_{CAS}$ data already increase during the *Lejopyge armata* biozone culminating in three positive excursions prior and after the SPICE maximum. Differences in onset, peak values and shape of the $\delta^{13}C_{carb}$ and/or $\delta^{34}S_{CAS}$ excursions at Kyrshabakty, but also in almost all sections characterized by the SPICE, are pointing towards Furongian seawater that was low in sulphate concentration and heterogeneous in its carbonate carbon and sulphate sulphur isotopic composition. The occurrence of benthic faunal elements in almost all SPICE-related sections strongly supports oxygenated conditions at the seafloor, therefore excluding widespread anoxia or euxinia. Regional anoxic conditions are most probable. A positive $\delta^{18}O_{carb}$ excursion parallel to the SPICE could probably be explained by a decline in seawater pH associated with a sea-level rise. Again, no euxinic conditions would be mandatory for explaining the SPICE event.

Keywords: Cambrian, SPICE, sulphur, carbon, oxygen, Kazakhstan.

1. Introduction

The Cambrian Period is characterized by four positive and six negative excursions in the marine $\delta^{13}C$ record that were related to eustatic sea-level changes, perturbations in the oceanic carbon cycle and, as a consequence, extinctions and evolutionary radiations in the Cambrian fauna (Peng *et al.* 2004; Babcock *et al.* 2005; Zhu, Babcock & Peng, 2006; Peng, Babcock & Cooper, 2012). One of the prominent positive excursions, the Steptoean positive carbon isotope excursion (SPICE), is situated at the base of the Paibian Stage (Furongian Series; Saltzman, Runnegar & Lohmann, 1998; Saltzman *et al.* 2000). It has been identified in carbonate and organic-rich successions of slope and platform environments of Antarctica, Argentina, Australia, England, Kazakhstan, Newfoundland, North and South China, Siberia, Sweden and the USA (e.g. Glumac & Walker, 1998; Saltzman, Runnegar & Lohmann, 1998; Saltzman *et al.* 2000, 2011; Peng *et al.* 2004; Zhu *et al.* 2004; Lindsay *et al.* 2005; Gill, Lyons & Saltzman, 2007; Gill *et al.* 2011; Kouchinsky *et al.* 2008; Sial *et al.* 2008, 2013; Ahlberg *et al.* 2009; Hurtgen, Pruss & Knoll, 2009; Chen *et al.* 2011, 2012; Woods *et al.* 2011; Ng, Yuan & Lin, 2014). In carbonate successions the SPICE is characterized by a shift of +4 ‰ to +6 ‰ in $\delta^{13}C_{carb}$ to peak values of about +5 ‰ (Saltzman *et al.* 2000; Woods *et al.* 2011). A similar positive excursion was observed in organic-rich sequences where $\delta^{13}C_{org}$ values increase by up to 3 ‰, culminating in a maximum value of about −28 ‰ (Ahlberg *et al.* 2009; Woods *et al.* 2011). Stratigraphically, the SPICE is well calibrated by the first appearance date (FAD) of *Glyptagnostus reticulatus* (base of the Paibian Stage) below and the FAD of *Irvingella* species above the $\delta^{13}C_{carb}$ peak, therefore allowing its global correlation (Saltzman *et al.* 2000). Furthermore, in Laurentia its maximum peak broadly coincides with: (1) the Sauk II – Sauk III hiatus (Palmer, 1981; Saltzman *et al.* 2000, 2004) as well as (2) a distinct maximum in the biotic diversity in the Pterocephaliid biomere boundary (Rowell & Brady, 1976; Saltzman *et al.* 2000; Peng *et al.* 2004).

A multitude of interpretations of the SPICE event exists considering increased weathering of terrestrial material or marine ^{13}C-enriched carbonates, leading to an increased burial of ^{12}C-enriched organic carbon under anoxic/euxinic conditions or enhanced

†Author for correspondence: thomas.wotte@uni-koeln.de

sedimentation rates, respectively (Kump *et al.* 1999; Kump & Arthur, 1999; Saltzman, Runnegar & Lohmann, 1998; Saltzman *et al.* 2000, 2004; Gill, Lyons & Saltzman, 2007; Hurtgen, Pruss & Knoll, 2009). Each of these processes would result in a more positive $\delta^{13}C$ signature of ambient seawater. However, the driving mechanisms behind the event are still poorly understood.

Considering the SPICE event as a consequence of weathering and changes in sea-level and climate, further changes in seawater chemistry (other than the perturbation of the global carbon cycle) should have occurred. Indeed, ^{87}Sr-enriched Sr isotope values are typical for the Furongian, indicating increased rates of erosion and continental silicate weathering (Montañez *et al.* 1996, 2000; Denison *et al.* 1998; Kouchinsky *et al.* 2008). In addition, the SPICE is often associated with positive excursions in the sulphur isotopic composition of carbonate-associated sulphate ($\delta^{34}S_{CAS}$) and sedimentary pyrite (i.e. chromium-reducible sulphur; $\delta^{34}S_{CRS}$) (Gill, Lyons & Saltzman, 2007; Hurtgen, Pruss & Knoll, 2009; Gill *et al.* 2011). The coupling of paired carbon and sulphur isotope trends is interpreted to reflect an elevated rate of organic carbon and pyrite burial during widespread euxinic conditions in Furongian oceans (Gill, Lyons & Saltzman, 2007; Gill *et al.* 2011). Carbon and sulphur isotope mass-balance models further indicate that the positive excursions in $\delta^{13}C$ and $\delta^{34}S$ are associated with a significant rise in the atmospheric O_2 level (Saltzman *et al.* 2011).

2. Geological setting

The Karatau Range of southern Kazakhstan represents the north-western prolongation of the Tien Shan Mountains, situated between the Chu-Sarysu Basin in the northeast and the Syrdarya Basin in the southwest (Alexeiev *et al.* 2009; Fig. 1a). It is separated into the north-western Bolshoi (Greater) Karatau and the south-eastern Malyi (Lesser) Karatau ranges. Fossiliferous Cambrian – Early Ordovician carbonate deposits of the Malyi Karatau Range were accumulated on the seaward prograding margin of an isolated carbonate platform which belongs to the Aisha-Bibi seamount (width of the mount *c.* 40 km; Cook *et al.* 1991; Saltzman *et al.* 2000; Ergaliev *et al.* 2009). The carbonate succession is exposed in several fault-bounded blocks and shows no or only minor tectonic dislocation (Holmer *et al.* 2001; Alexeiev *et al.* 2009).

The Kyrshabakty section is situated at the Kyrshabakty river, *c.* 20 km east of the town of Zhanatas (Fig. 1b). The base of the more than 600-m-thick succession is located at 43° 32′ 02″ N and 69° 57′ 28″ E at an elevation of *c.* 500 m. Coordinates of the section have been previously misdated by Ergaliev *et al.* (2009) and Peng *et al.* (2012) as located northeast of Zhanatas at a longitude of 69° 51′ 28″ E. The section was investigated under multiple aspects, encompassing detailed analyses on litho- (Cook, *et al.* 1991) and biofacies (Holmer *et al.* 2001; Ergaliev, 1980, 1981, 1992; Ergaliev & Ergaliev, 2004, 2008) and carbon isotopes (Saltzman *et al.* 2000). Several concepts for a litho- and biostratigraphic subdivision exist for the Kyrshabakty section, which have been significantly modified during the last three decades (for more information see Ergaliev, 1980; Holmer *et al.* 2001; Ergaliev & Ergaliev, 2008; Ergaliev *et al.* 2009). Here, we apply the most recent trilobite zonation (Ergaliev *et al.* 2009) and the subdivision of the sedimentary succession into informal lithostratigraphic units (units I–XII) as established by Ergaliev (1980). At Kyrshabakty, only 9 (units IV–XII) of the 12 informal units are exposed. The basal units IV and V (up to 100 m in thickness) are composed of dark laminated argillaceous limestone, limestone and carbonate claystone representing a basin-plain environment (Fig. 2). Upsection, units VI–XI (*c.* 490 m in thickness) are dominated by dark laminated limestone, nodular limestone and carbonate breccias, interpreted as turbidites of carbonate submarine fan deposits (Fig. 2). Grey to brown dolostone, dolomitic limestone and (partly oolitic) limestone are exposed in unit XII, and reflect a shallow-subtidal lagoonal or tidal-flat environment. According to Cook *et al.* (1991), Ergaliev & Ergaliev (2008) and Ergaliev *et al.* (2009), the sedimentary succession of Kyrshabakty section was accumulated on the north-eastern flank (recent orientation) of the Aisha-Bibi seamount. It covers the stratigraphic interval ranging from the undefined Cambrian Series 3/Stage 5 (uppermost *Peronopsis ultimus* zone, known as 'Lenan' Stage in Kazakh nomenclature; Geyer & Shergold, 2000; Ergaliev *et al.* 2009) to the Furongian Series/undefined Stage 10 (*Micragnostus mutabilis-Lophosaukia* zones, known as Batyrbaian Stage of the Kazakh nomenclature; Ergaliev *et al.* 2009).

Within the interval covering the *Glyptagnostus stolidotos* to *Pseudagnostus vastulus-Irvingella tropica* trilobite zones (informal units VII and VIII), the SPICE event was identified by Saltzman *et al.* (2000).

Here, we present the sulphur isotope values of carbonate-associated sulphate ($\delta^{34}S_{CAS}$) and chromium-reducible sulphur ($\delta^{34}S_{CRS}$) of 58 carbonate samples of the Kyrshabakty section, covering the middle Drumian–Jiangshanian stages (Fig. 2). In addition, samples were analysed for their carbonate carbon ($\delta^{13}C_{carb}$) and oxygen ($\delta^{18}O_{carb}$) isotopes, and their elemental concentrations (Ca, Fe, Mg, Mn and Sr). This extensive dataset provides the unusual opportunity to study the relationships between marine carbon and sulphur cycles in context with environmental, biological and climate changes during Furongian time. From chemostratigraphic studies and an in-depth evaluation of the biostratigraphic constraints, we try to unravel the processes and conditions which forced the parallel excursions in $\delta^{13}C$ and $\delta^{34}S$ during the SPICE interval.

3. Material and methods

Sample preparation and analytical work were conducted in the laboratories of the universities of Münster and Kiel using standard procedures. In a first step,

https://doi.org/10.1017/S0016756815000187 Published online by Cambridge University Press

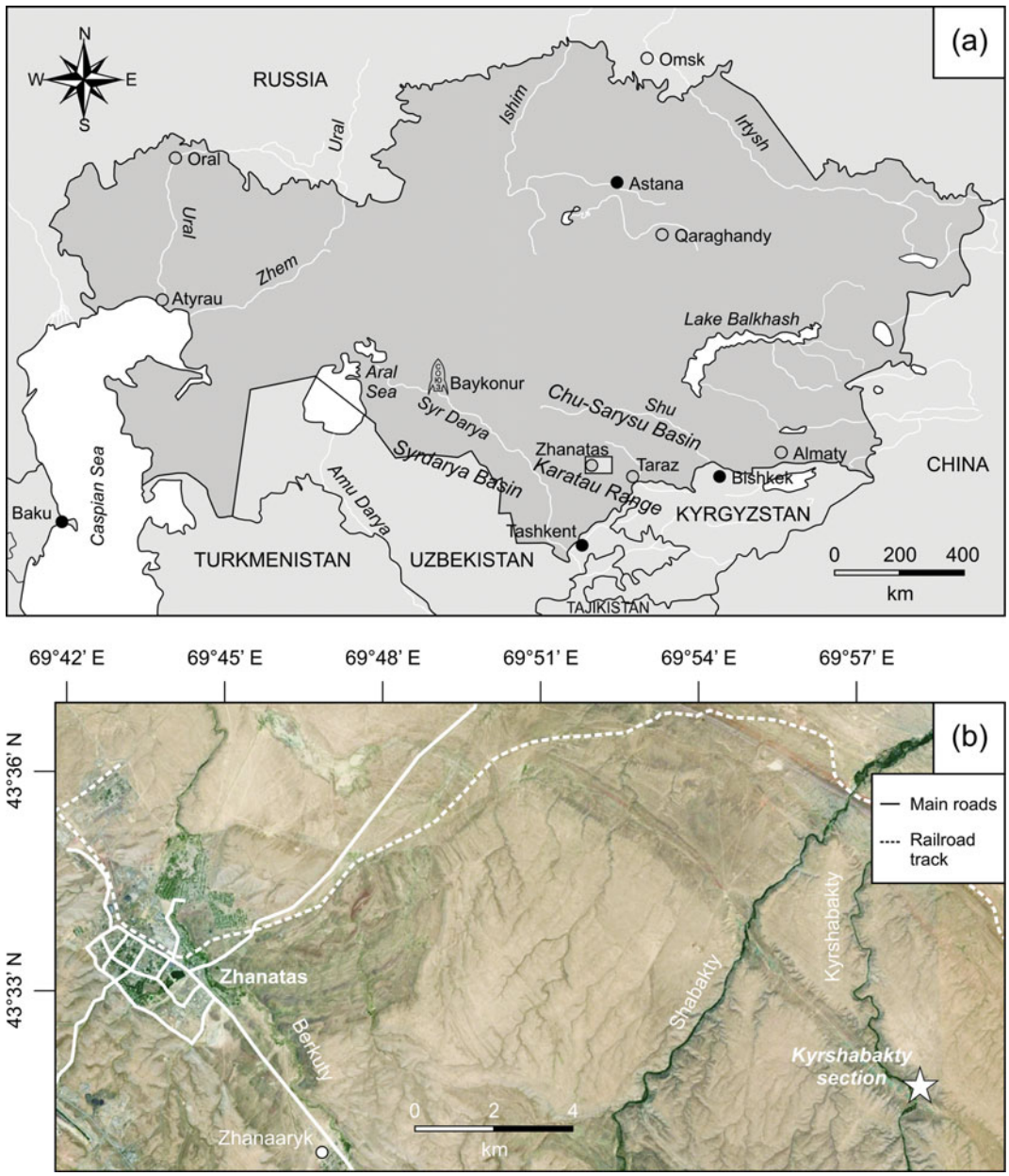

Figure 1. (Colour online) (a) Simplified map of Kazakhstan. The grey square marks the location of the working area in the surroundings of Zhanatas (southern Kazakhstan). (b) Map of the working area showing the topographic position of Kyrshabakty section (based on Google Earth, December 2014).

contaminations such as calcite veins or weathering crusts were removed. Bulk-rock samples were subsequently powdered to <63 μm using a tungsten carbide ring and puck mill, delivering whole-rock material for isotope and element analyses.

$\delta^{13}C_{carb}$ and $\delta^{18}O_{carb}$ analyses were performed automatically using a GasBench II connected via a ConFlow-II Interface to a Finnigan MAT DeltaPlusXL. Delta values are reported relative to the V-PDB standard. The analytical reproducibility was generally better than 0.1 ‰ for $\delta^{13}C_{carb}$ and 0.2 ‰ for $\delta^{18}O_{carb}$.

Extraction of carbonate-associated sulphate (CAS) from carbonate rocks was performed by applying the rigid extraction protocol of Wotte, Shields-Zhou & Strauss, (2012) and Wotte *et al.* (2012), known to deliver the most accurate $\delta^{34}S_{CAS}$ values. Up to 694 g per sample was used to analyse CAS concentration and isotopic composition (Table 1). In addition to the CAS extraction, the concentration and isotopic composition of chromium-reducible sulphur (CRS or pyrite sulphur) were determined. Analyses of CRS are essential in order to obtain information about alteration of CAS due to sulphate oxidation and/or bacterial sulphate reduction (Wotte, Strauss & Sundberg, 2011; Wotte, Shields-Zhou & Strauss, 2012; Wotte *et al.* 2012). CRS was extracted from 0.8–37.7 g of dried insoluble residue subsequent to CAS extraction, basically following the extraction procedure described by Canfield *et al.* (1986). $\delta^{34}S_{CAS}$ and $\delta^{34}S_{CRS}$ were measured using a Thermo-Finnigan Delta Plus mass spectrometer connected to an Elemental Analyser (EA-IRMS). Results are reported in the usual delta notation as per mil (‰)

https://doi.org/10.1017/S0016756815000187 Published online by Cambridge University Press

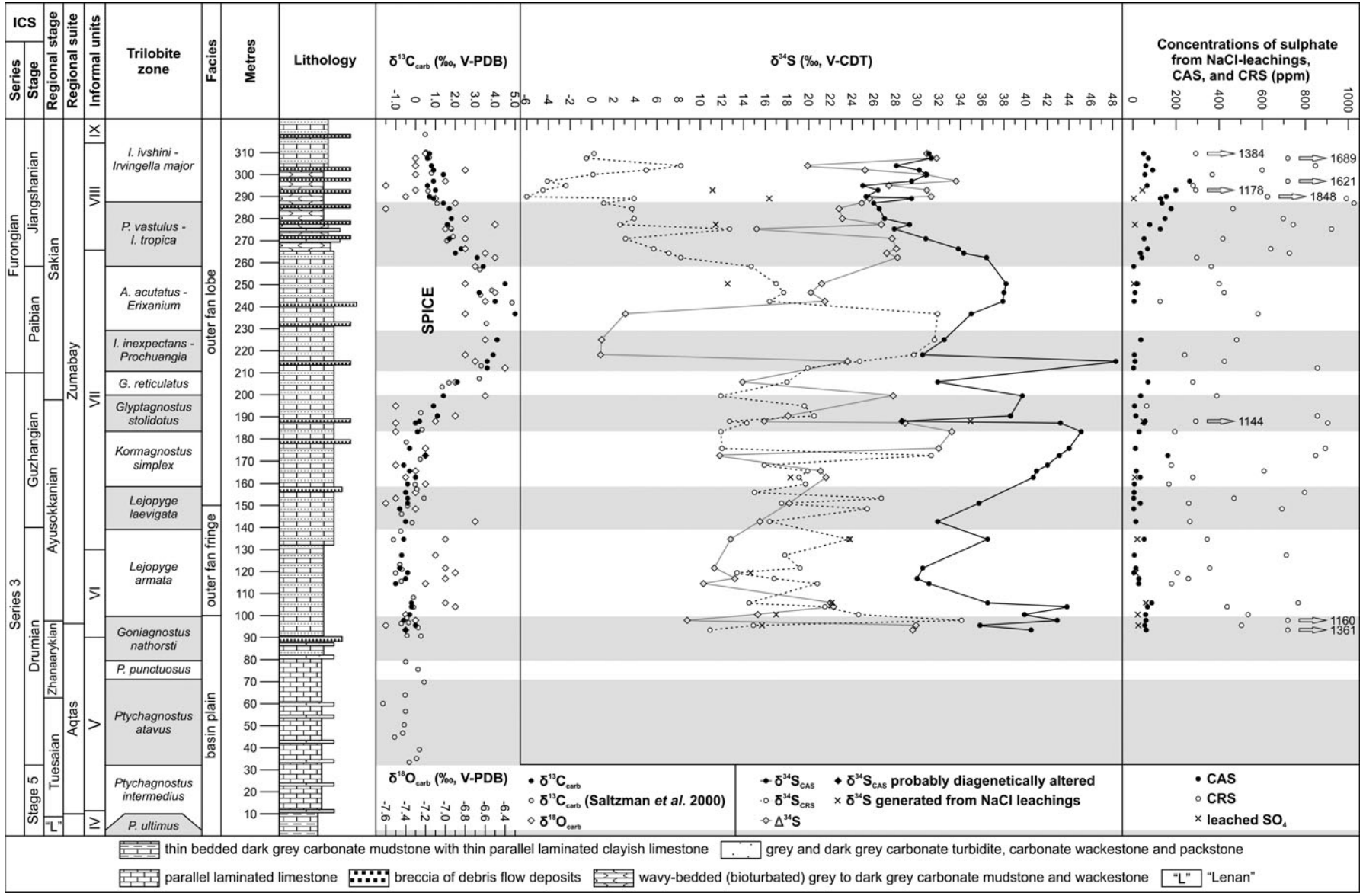

Figure 2. Stratigraphic column and geochemical data for the Kyrshabakty section (southern Kazakhstan). Placement of international and regional stratigraphic subdivision is based on Ergaliev & Ergaliev (2008), Ergaliev *et al.* (2009) and Geyer & Shergold (2000). *A. acutatus* – *Acutatagnostus acutatus*; *G. reticulatus* – *Glyptagnostus reticulatus*; *I. inexpectans* – *Innitagnostus inexpectans*; *I. tropica* – *Irvingella tropica*; *I. ivshini* – *Ivshinagnostus ivshini*; *P. ultimus* – *Peronopsis ultimus*; *P. vastulus* – *Pseudagnostus vastulus*; *P. punctuosus* – *Ptychagnostus punctuosus*.

Table 1. Isotopic and elemental composition and initial weights for CAS and CRS analyses of samples from Kyrshabakty section.

Sample	Meters (m)	$\delta^{13}C_{carb}$ (‰, V-PDB)	$\delta^{18}O_{carb}$ (‰, V-PDB)	Weight for CAS analyses (g)	$\delta^{34}S_{CAS}$ (‰, V-CDT)	CAS (ppm)	Weight for CRS analyses (g)	$\delta^{34}S_{CRS}$ (‰, V-CDT)	CRS (ppm)	$\Delta^{34}S$ (‰, V-CDT)	Fe (ppm)	Mn (ppm)	Mg (ppm)	Ca (ppm)	Sr (ppm)	Mn/Sr	Ca/Mg
K1	93.5	−0.5	−7.4	274	40.5	62	21.0	10.9	1361	29.6	37	137	2872	366978	634	0.22	128
K2	95.6	0.0	−7.6	431	35.8	55	26.7	14.9	503	20.9	65	201	3270	374394	707	0.28	115
K3	97.9	−0.6	−7.3	621	42.9	61	17.2	34.1	1160	8.8	37	245	2579	318288	640	0.38	123
K4	100.5	−0.3	−7.4	427	39.9	59	22.2	24.6	534	15.3	84	324	2568	364408	545	0.59	142
K5	104.0	−0.2	−6.9	143	43.8	68	11.4	21.5	437	22.3	63	146	3471	379629	610	0.24	109
K6	105.7	−0.2	−7.0	537	36.5	88	20.7	14.5	766	22.0	36	113	2737	365471	490	0.23	134
K7	114.5	−1.0	−7.2	467	31.1	27	34.5	20.8	179	10.3	60	304	1698	356977	311	0.98	210
K8	116.8	−0.5	−7.0	335	30.0	28	13.3	16.8	257	13.2	42	73	2090	342232	388	0.19	164
K9	119.4	−0.4	−6.9	522		5	21.1	13.4	206		109	263	1954	366728	364	0.72	188
K10	121.5	−0.8	−7.0	383	30.5	14	7.5	19.2	356	11.3	58	209	1764	369824	356	0.59	210
K11	127.4	−0.7	−7.1	263		7	10.6	17.8	711		63	81	2259	374538	552	0.15	166
K12	134.6	−0.6	−7.0	626	36.5	52	26.1	23.7	344	12.8	90	82	2692	366230	391	0.21	136
K13	142.6	−0.5	−6.7	461	31.9	14	37.7	16.4	264	15.5	63	72	1825	364771	303	0.24	200
K14	148.4	−0.8	−7.3	169		4	5.8	25.4	691		50	96	2684	376608	439	0.22	140
K16	150.9	−0.4	−7.6	509	35.7	34	20.8	17.5	259	18.2	147	85	2192	365900	602	0.14	167
K15	153.2	−0.4	−7.5	610		4	20.3	26.7	469		99	104	1573	366684	423	0.25	233
K17	155.9	−0.5	−7.3	609		6	17.8	15.0	796		75	61	2371	365136	613	0.10	154
K18	159.6	−0.4	−7.2	549		7	28.0	19.7	167		127	94	2014	365387	590	0.16	181
K19	162.7	0.0	−7.4	464	40.7	34	18.2	19.1	278	21.6	78	99	2068	380009	430	0.23	184
K20	165.6	−0.3	−7.3	594	41.0	16	17.6	19.9	608	21.1	99	114	2711	364274	560	0.20	134
K21	168.2	−0.6	−7.5	287	42.0	112	25.3	15.9	178		153	159	1906	338091	438	0.36	177
K22	172.4	0.5	−7.2	260	43.1	162	9.7	31.3	847	11.8	78	86	2835	366648	531	0.16	129
K23	175.6	−0.3	−7.2	215	44.0	12	14.7	12.0	892	32.0	122	477	2338	358209	428	1.11	153
K24	183.1	0.1	−7.5	253	45.1	29	27.5	11.9	194	33.2	221	163	1762	363463	564	0.29	206
K25	187.1	0.0	−7.5	485	43.2	52	17.3	14.3	904	28.9	98	403	2145	362156	431	0.94	169
K26	187.9	0.2	−7.1	473	28.6	57	22.3	12.7	1144	15.9	200	375	2180	344647	314	1.19	158
K27	190.3	1.1	−6.9	603	38.6	14	14.3	20.5	855	18.1	41	197	2521	372281	382	0.52	148
K28	194.8	0.9	−7.5	178		8	18.3	19.6	64		195	783	2483	355625	386	2.03	143
K29	199.4	1.4	−6.6	694	39.7	36	20.8	11.9	389	27.8	36	209	2470	372299	385	0.54	151
K30	205.7	2.1	−6.9	377	31.9	70	10.7	18.0	278	13.9	40	110	2545	369723	441	0.25	145
K31	212.0	3.6	−6.4	618		3	14.7	19.9	855		35	27	3417	365626	535	0.05	107
K32	215.0	3.6	−6.7	226	48.3	10	5.6	24.7	424	23.6	39	40	2413	374324	520	0.08	155
K33	218.0	3.9	−6.8	258	30.5	7	13.7	29.7	240	0.8	47	56	2320	379159	920	0.06	163

Table 1. Continued.

Sample	Meters (m)	$\delta^{13}C_{carb}$ (‰, V-PDB)	$\delta^{18}O_{carb}$ (‰, V-PDB)	Weight for CAS analyses (g)	$\delta^{34}S_{CAS}$ (‰, V-CDT)	CAS (ppm)	Weight for CRS analyses (g)	$\delta^{34}S_{CRS}$ (‰, V-CDT)	CRS (ppm)	$\Delta^{34}S$ (‰, V-CDT)	Fe (ppm)	Mn (ppm)	Mg (ppm)	Ca (ppm)	Sr (ppm)	Mn/Sr	Ca/Mg
K34	224.9	4.1	− 6.6	315	32.5	37	11.6	31.6	481	0.9	44	40	2295	369002	827	0.05	161
K41	236.6	5.0	− 6.8	575	35.0	54	22.3	31.9	580	3.1	43	61	2871	375192	906	0.07	131
K42	242.3	4.0	− 6.6	293	37.9	16	23.1	16.4	126	21.5	40	26	2547	358148	644	0.04	141
K39	246.2	3.2	− 6.5	216	38.0	10	3.0	17.7	423	20.3	42	28	2765	370028	562	0.05	134
K40	250.3	4.5	− 6.8	553	38.2	21	4.1	17.0	400	21.2	120	56	3020	377299	603	0.09	125
K38	258.1	3.4	− 6.7	42		4	0.8	14.7	363		36	61	2440	328524	454	0.13	135
K37	262.1	3.1	− 6.5	343	36.4	42	30.6	8.2	296	28.2	65	78	3455	382210	561	0.14	111
K36	264.1	2.0	− 6.6	556	34.3	35	20.2	7.1	724	27.2	39	71	1759	381772	367	0.19	217
K35	266.1	2.3	− 6.8	271	33.8	68	3.2	5.7	639	28.1	44	94	2373	372291	389	0.24	157
K43	270.7	1.7	− 6.8	324	30.8	52	7.8	3.1	417	27.7	41	60	3441	382946	482	0.13	111
K44	275.1	1,8	− 7.0	623	27.9	127	6.8	12.7	920	15.2	61	49	2323	335119	344	0.14	144
K45	277.1	1.6	− 6.5	520	29.3	78	17.0	2.6	743	26.7	57	47	3411	365151	398	0.12	107
K46	279.8	1.8	− 6.8	416	27.0	149	13.3	3.9	697	23.1	90	60	2785	369295	354	0.17	133
K48	284.3	1.7	− 7.6	258	26.5	177	21.0	3.7	464	22.8	235	108	2656	361620	379	0.28	136
K47	286.8	1.4	− 6.9	237	26.0	150	5.4	1.1	1025	24.9	76	53	3088	372059	434	0.12	120
K49	288.9	0.9	− 7.1	584	29.5	128	10.7	3.9	990	25.6	223	83	2302	357102	315	0.26	155
K50	289.8	0.7	− 7.4	89	25.3	150	2.2	− 6.0	1848	31.3	47	104	2587	357934	292	0.36	138
K50/1	292.7	1.0	− 7.3	568	26.4	199	14.7	− 4.5	1178	30.9	131	109	2401	360901	307	0.35	150
K53	294.8	0.6	− 7.6	452	25.0	66	21.4	− 2.4	279	27.4	186	126	2506	329026	320	0.39	131
K52	296.8	0.9	− 7.0	308	29.5	263	6.6	− 4.1	1621	33.6	67	45	2492	349471	294	0.15	140
K51	299.8	1.4	− 7.3	628	30.9	56	25.7	0.1	368	30.8	266	52	2205	346894	427	0.12	157
K54	301.8	0.9	− 6.8	85	30.2	92	12.5	5.0	600	25.2	36	61	3124	361939	388	0.16	116
K55	303.8	0.8	− 7.3	627	28.1	60	7.8	8.2	847	19.9	40	42	2944	370454	359	0.12	126
K56	307.2	0.6	− 7.3	310	31.3	72	2.7	− 0.5	1689	31.8	139	32	2759	351500	361	0.09	127
K57	309.3	0.7	− 7.2	588	31.1	50	6.8	0.2	1384	30.9	83	55	2804	371440	349	0.16	132

difference to the V-CDT standard. Reproducibility was better than ±0.3 ‰.

In order to evaluate carbonate diagenesis, elemental concentrations (Ca, Fe, Mg, Mn and Sr) were measured (Wotte, Strauss & Sundberg, 2011; Wotte, Shields-Zhou & Strauss, 2012; Wotte *et al.* 2012). Subsequent to the reaction of 1 g of sample material with 20 mL of acetic acid (2 %), suspension was filtered after 48 hours of reaction time. The filtrate was analysed for their elemental abundances by simultaneous inductively coupled plasma optical emission spectrometry (ICP-OES, SPECTRO CIROS SOP) after calibration with matrix-matched standards. Analytical precision was better than 0.5 %. Accuracy was monitored by the analysis of USGS MAG-1 standard and found to be within 1 % of recommended values (GeoReM online data base). Elemental concentrations were corrected for the insoluble residue and are reported in ppm.

4. Results

$\delta^{13}C_{carb}$ data vary between −1.0 ‰ and +0.5 ‰ within the informal units VI and VII (*Goniagnostus nathorsti – Glyptagnostus stolidotos* zones), increase within the *Glyptagnostus stolidotos* and *Innitagnostus inexpectans-Prochuangia* biozones (middle–upper part of unit VII) towards +4.1 ‰, and finally reach a maximum value of +5.0 ‰ in the lower *Acutatagnostus acutatus-Erixanium* biozone (upper part of unit VII) (Fig. 2; Table 1). Subsequently, $\delta^{13}C_{carb}$ values continuously decrease upsection, reaching a minimum of +0.6 ‰ (sample K56) at the top of the measured section. The establishment of a new baseline after the prominent excursion is discernible with post-excursion $\delta^{13}C_{carb}$ values of *c.* 1–3 ‰ more positive than data prior to the excursion.

An almost identical trend is described by the $\delta^{18}O_{carb}$ data, increasing from minimum values of −7.6 ‰ towards a maximum of −6.5 ‰ within the *Glyptagnostus stolidotos* to the *Acutatagnostus acutatus-Erixanium* biozones (Fig. 2; Table 1). The data continuously decrease towards a minimum of −7.6 ‰ near the top of the section.

CAS concentrations vary between 3 ppm and 263 ppm (Fig. 2; Table 1). Respective $\delta^{34}S_{CAS}$ values range from 25.0 ‰ to 48.3 ‰ showing two distinctive positive excursions within the lower part of unit VII (*Kormagnostus simplex – Glyptagnostus stolidotos* biozones; maximum 45.1 ‰ at K24) and the upper part of unit VII – basal unit VIII (*Acutatagnostus acutatus-Erixanium* to *Pseudagnostus vastulus-Irvingella tropica* biozones; maximum 38.2 ‰ at K40). Both positive trends are separated by a few data points exhibiting a high variability between 28.6 ‰ (K26) and 48.3 ‰ (K32). Starting from the second positive excursion (38.2 ‰ at K40), $\delta^{34}S_{CAS}$ values decrease rapidly, culminating in a minimum of 25.0 ‰ (Fig. 2; Table 1). $\delta^{34}S_{CRS}$ data fluctuate between −6.0 ‰ at the top and 34.1 ‰ at the base of the succession. $\delta^{34}S_{CRS}$ of the lower part of the section (up to the base of the *Glyptagnostus reticulatus* zone) vary between 10.9 ‰ and 34.1 ‰. A subsequent increase in $\delta^{34}S_{CRS}$ values culminates in a maximum peak of 31.9 ‰ (basal *Acutatagnostus acutatus-Erixanium* biozone) followed by a rapid drop to −6.0 ‰ (Fig. 2; Table 1). Corresponding CRS concentrations range from 126 ppm to 1848 ppm with no clear stratigraphic trend. Calculated $\Delta^{34}S$ values ($\delta^{34}S_{CAS} - \delta^{34}S_{CRS}$) range from 0.8 ‰ to 33.6 ‰ (Fig. 2; Table 1). The post-excursion $\delta^{34}S_{CAS}$ and $\delta^{34}S_{CRS}$ baselines are significantly less positive than the sulphur isotope values before the events (Fig. 2). Upsection, both curves show a principle trend in $\delta^{34}S$ towards less positive values.

Elemental concentrations show no major variation across the succession with values of 35–266 ppm for Fe, 26–783 ppm for Mn, 1573–3471 ppm for Mg, 292–920 ppm for Sr and 31.8–38.3 wt % for Ca (Table 1).

5. Diagenetic constraints

Prior to interpreting the carbon and sulphur isotopes, an evaluation of the degree of post-depositional alteration is essential. Respective proxies include $\delta^{18}O_{carb}$ values and elemental abundances and ratios (especially of Ca, Fe, Mg, Mn and Sr) of the carbonate matrix (Brand & Veizer, 1980; Veizer *et al.* 1999; Wotte, Strauss & Sundberg, 2011; Wotte, Shields-Zhou & Strauss, 2012; Wotte *et al.* 2012). Samples characterized by $\delta^{18}O_{carb} > -10.0$ ‰ and a Mn/Sr < 10 (or even < 2–3) are frequently considered as representing a diagenetically well-preserved isotopic signal (Kaufman, Jacobsen & Knoll, 1993; Kaufman & Knoll, 1995). Our carbonate samples display $\delta^{18}O_{carb}$ values more positive than −10.0 ‰ and an Mn/Sr of <3 (Figs 3a–d, 4a–b; Table 1). Furthermore, Ca/Mg is regarded as a proxy signal for determining the effect of dolomitization, with Ca/Mg >50 considered as representing carbonate samples with the least-altered $\delta^{34}S_{CAS}$ values (Marenco *et al.* 2008). Our Ca/Mg is generally above 50, indicating no or only minor diagenetic alteration of sampled material (Fig. 3c, e, f; Table 1).

In order to evaluate a post-depositional resetting of the primary marine isotope signal, cross-plots of seawater proxies versus proxies of diagenetic alteration are applied (Banner & Hanson, 1990; Jacobsen & Kaufman, 1999; Wotte *et al.* 2007; Derry, 2010; Gill *et al.* 2011). Plots using a combination of $\delta^{13}C_{carb}$, $\delta^{18}O_{carb}$, Mn/Sr and Ca/Mg show no covariance, indicating the absence of any substantial post-depositional carbonate alteration and the corresponding isotope data (Figs. 3, 4). In addition, no correlations exist between the proxies of diagenesis versus CAS and CRS concentrations and/or their sulphur isotope compositions (Figs 3, 4). We therefore assume that a severe and/or heterogeneous alteration of our carbonate samples is absent.

Caution needs to be applied when considering the quality of isotopic values and concentrations of CAS and CRS. Prior to the final liberation of CAS from the carbonate lattice it is essential to eliminate all

https://doi.org/10.1017/S0016756815000187 Published online by Cambridge University Press

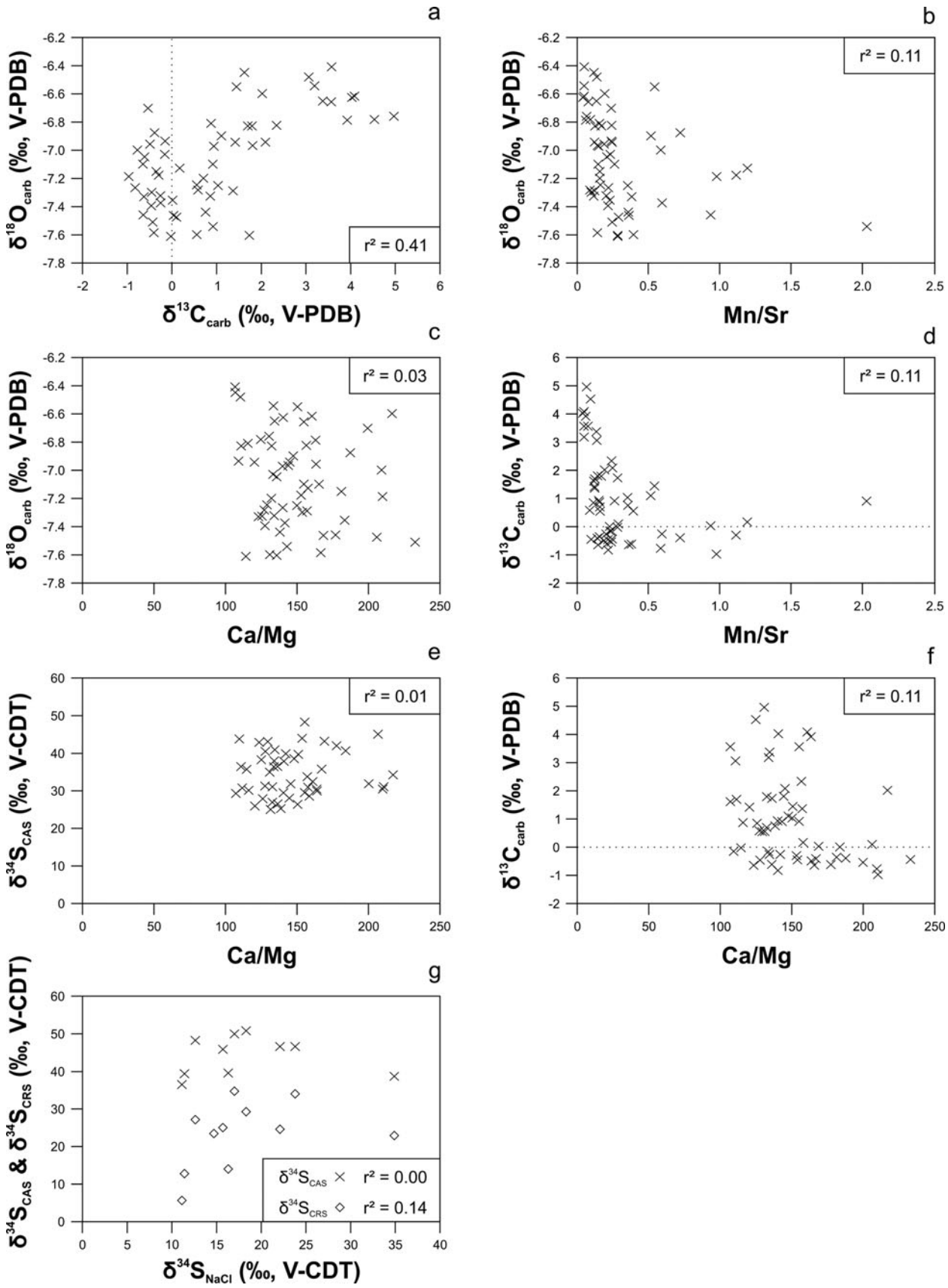

Figure 3. Cross-plots of stable isotope data, CAS and CRS concentrations, and element data from Kyrshabakty section. No covariance between proxies of diagenesis versus stable isotopes indicates the absence of any alteration of sample material and corresponding isotope data. (a) $\delta^{18}O_{carb}$ (‰, V-PDB) against $\delta^{13}C_{carb}$ (‰, V-PDB). (b) $\delta^{18}O_{carb}$ (‰, V-PDB) against Mn/Sr. (c) $\delta^{18}O_{carb}$ (‰, V-PDB) against Ca/Mg. (d) $\delta^{13}C_{carb}$ (‰, V-PDB) against Mn/Sr. (e) $\delta^{34}S_{CAS}$ (‰, V-CDT) against Ca/Mg. (f) $\delta^{13}C_{carb}$ (‰, V-PDB) against Ca/Mg. (g) $\delta^{34}S_{CAS}$ (‰, V-CDT) and $\delta^{34}S_{CRS}$ (‰, V-CDT) against $\delta^{34}S_{NaCl}$ (‰, V-CDT). $\delta^{34}S_{NaCl}$ values differ from the $\delta^{34}S_{CAS}$ and $\delta^{34}S_{CRS}$ data, indicating no influence of the non-CAS fraction on the final CAS and CRS isotopic values.

https://doi.org/10.1017/S0016756815000187 Published online by Cambridge University Press

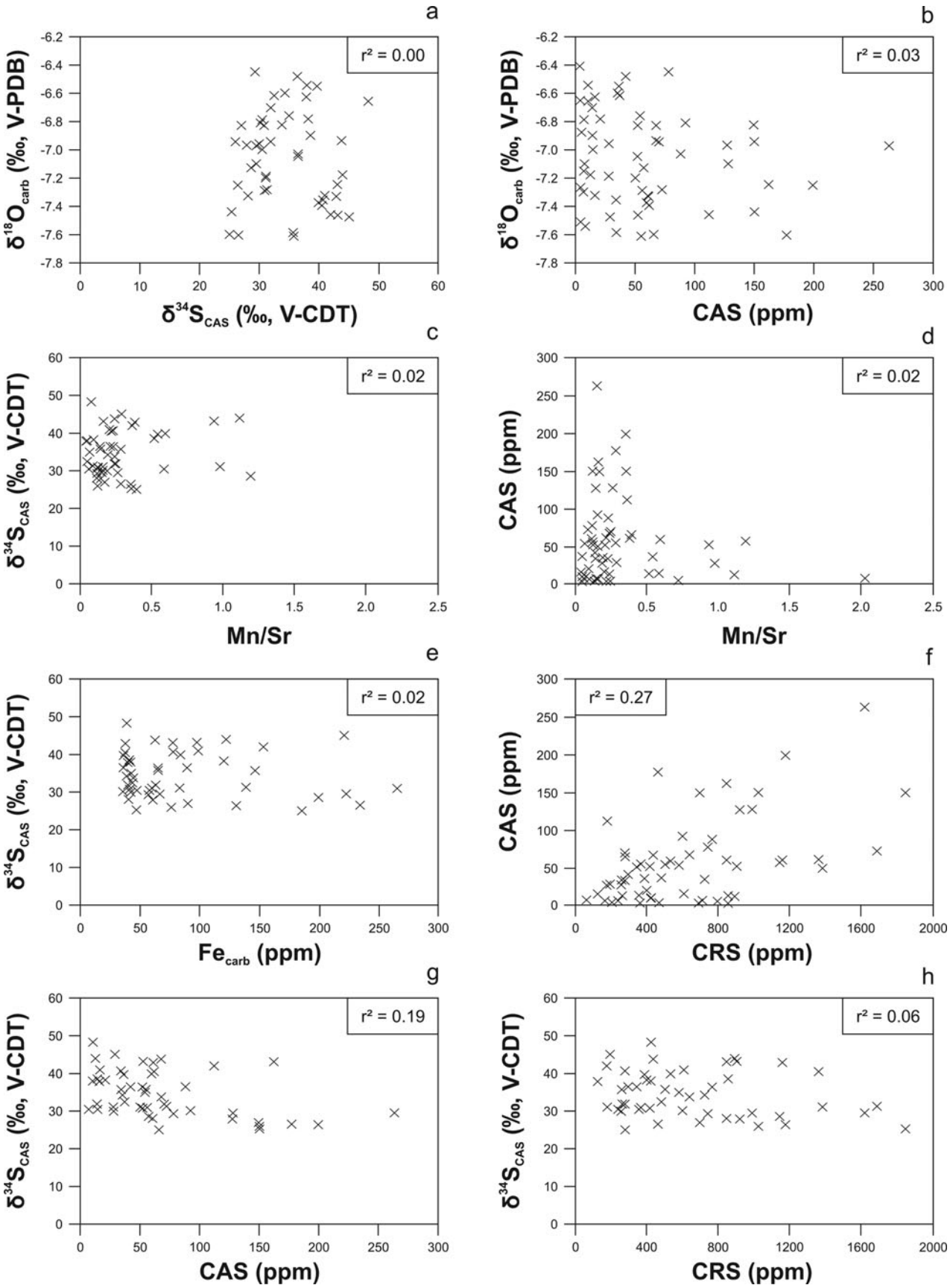

Figure 4. Cross-plots of stable isotope data, CAS and CRS concentrations, and element data from Kyrshabakty sections. The absence of any correlation between $\delta^{34}S_{CAS}$, CAS and proxies for diagenesis suggests that the sulphur isotopic composition of carbonate-associated sulphate was not diagenetically altered. (a) $\delta^{18}O_{carb}$ (‰, V-PDB) against $\delta^{34}S_{CAS}$ (‰, V-CDT). (b) $\delta^{18}O_{carb}$ (‰, V-PDB) against CAS (ppm). (c) $\delta^{34}S_{CAS}$ (‰, V-CDT) against Mn/Sr. (d) CAS (ppm) against Mn/Sr. (e) $\delta^{34}S_{CAS}$ (‰, V-CDT) against Fe_{carb} (ppm). (f) CAS (ppm) against CRS (ppm). (g) $\delta^{34}S_{CAS}$ (‰, V-CDT) against CAS (ppm). (h) $\delta^{34}S_{CAS}$ (‰, V-CDT) against CRS (ppm).

https://doi.org/10.1017/S0016756815000187 Published online by Cambridge University Press

leachable non-CAS sulphur-bearing phases (Kampschulte, Bruckschen & Strauss, 2001; Kampschulte & Strauss, 2004; Wotte, Strauss & Sundberg, 2011; Wotte, Shields-Zhou & Strauss, 2012; Wotte *et al.* 2012). A consecutive leaching procedure with 10 % NaCl (aq) is therefore considered as delivering the most pristine CAS and CRS concentrations and isotopic compositions (for more information see Wotte *et al.* 2012). Although no leachable non-CAS was detected for 47 out of the 58 samples after the first NaCl-leaching, double leaching was necessary for 11 samples in order to eliminate all non-CAS compounds (Table 2) from the sample powder. $\delta^{34}S_{NaCl}$ values vary between 11.1 ‰ (K50/1) and 34.9 ‰ (K26) with concentrations between 2 ppm (K9) and 67 ppm (K6). These values clearly differ from the $\delta^{34}S_{CAS}$ and $\delta^{34}S_{CRS}$ data, indicating no influence of the non-CAS fraction on the final CAS isotope values (Fig. 3g; Table 2).

Another aspect concerning CAS is that its abundance decreases during progressive diagenetic alteration, but with no influence on the $\delta^{34}S_{CAS}$ data (Hurtgen *et al.* 2006; Gill, Lyons & Frank, 2008). It should be considered, however, that the primary $\delta^{34}S_{CAS}$ signal can only be affected by sulphate derived from either sulphide oxidation or bacterial sulphate reduction if that sulphate is incorporated into the carbonate (Kampschulte & Strauss, 2004; Wotte *et al.* 2012). The clearly less positive $\delta^{34}S_{CAS}$ value of sample K26 (28.6 ‰) correlates with enhanced CRS (1144 ppm) and Fe (200 ppm) concentrations, probably indicating an incorporation of sulphate derived from pyrite oxidation (Table 1). Considering the successive leaching with NaCl, oxidation must have happened during the diagenesis rather than represent an analytical artefact (Marenco *et al.* 2008). However, no covariance between less-positive $\delta^{34}S_{CAS}$ data and high CRS and/or Fe concentrations exist (Fig. 4e, h). For samples K30 and K33, separating the maximum $\delta^{34}S_{CAS}$ value (48.3 ‰ at K32) and the two distinctive positive excursions during the Guzhangian–Paibian interval, there is no correlation between the less positive $\delta^{34}S_{CAS}$ values (31.9 ‰ at K30 and 30.5 at K33) and enhanced CRS and/or Fe concentrations (Table 1). Regarding the arguments above, we consider our $\delta^{13}C_{carb}$, $\delta^{18}O_{carb}$, $\delta^{34}S_{CAS}$ and $\delta^{34}S_{CRS}$ data as reflecting the isotopic composition of ambient seawater. For further discussions on diagenetic alteration of $\delta^{34}S_{CAS}$ values see Wotte, Shields-Zhou & Strauss (2012) and Wotte *et al.* (2012).

Table 2. Comparison of $\delta^{34}S_{NaCl}$, $\delta^{34}S_{CAS}$ and $\delta^{34}S_{CRS}$ data, and SO_4 concentrations generated from NaCl leachings.

Sample	$\delta^{34}S_{NaCl}$ (‰, V-CDT)	SO_4 (ppm)	$\delta^{34}S_{CAS}$ (‰, V-CDT)	$\delta^{34}S_{CRS}$ (‰, V-CDT)
K1			40.5	10.9
K2	15.7	32	35.8	14.9
K3			42.9	34.1
K4	17.0	29	39.9	24.6
K5			43.8	21.5
K6	22.1	67	36.5	14.5
K7			31.1	20.8
K8			30.0	16.8
K9	14.7	2		13.4
K10			30.5	19.2
K11				17.8
K12	23.8	27	36.5	23.7
K13			31.9	16.4
K14				25.4
K16			35.7	17.5
K15				26.7
K17				15.0
K18				19.7
K19	18.3	6	40.7	19.1
K20			41.0	19.9
K21			42.0	15.9
K22			43.1	31.3
K23			44.0	12.0
K24			45.1	11.9
K25			43.2	14.3
K26	34.9	14	28.6	12.7
K27			38.6	20.5
K28				19.6
K29			39.7	11.9
K30			31.9	18.0
K31				19.9
K32			48.3	24.7
K33			30.5	29.7
K34			32.5	31.6
K41			35.0	31.9
K42			37.9	16.4
K39			38.0	17.7
K40	12.6	10	38.2	17.0
K38				14.7
K37			36.4	8.2
K36			34.3	7.1
K35			33.8	5.7
K43			30.8	3.1
K44			27.9	12.7
K45	11.4	6	29.3	2.6
K46			27.0	3.9
K48			26.5	3.7
K47			26.0	1.1
K49	16.3	11	29.5	3.9
K50			25.3	–6.0
K50/1	11.1	50	26.4	–4.5
K53			25.0	–2.4
K52			29.5	–4.1
K51			30.9	0.1
K54			30.2	5.0
K55			28.1	8.2
K56			31.3	–0.5
K57			31.1	0.2

6. Discussion

6.a. $\delta^{13}C_{carb}$ values: stratigraphic variations and biostratigraphic constraints

Our $\delta^{13}C_{carb}$ values of the Kyrshabakty section reproduce and extend the dataset of Saltzman *et al.* (2000). The $\delta^{13}C_{carb}$ peak value of +5.0 ‰ (+4.82 ‰ in Saltzman *et al.* 2000) is situated within the *Acutatagnostus acutatus-Erixanium* biozone and represents the maximum amplitude of the SPICE event (Fig. 2). The onset of the SPICE is generally considered as coinciding with the FAD of *Glyptagnostus reticulatus* (base of the Paibian; Peng *et al.* 2004). At the Kyrshabakty section, the evolution towards more positive $\delta^{13}C_{carb}$ values starts during the uppermost Guzhangian Stage (*Kormagnostus simplex* and *Glyptagnostus stolidotus* biozones; Fig. 2). A similar positive trend prior to the FAD of *G. reticulatus* is

https://doi.org/10.1017/S0016756815000187 Published online by Cambridge University Press

reported for the majority of sections (Australia, China, France, Nevada, Newfoundland, Sweden and UK) at which the SPICE has been identified (Saltzman *et al.* 2000; Gill, Lyons & Saltzman, 2007; Álvaro *et al.* 2008; Ahlberg *et al.* 2009; Hurtgen, Pruss & Knoll, 2009; Chen *et al.* 2011, 2012; Gill *et al.* 2011; Woods *et al.* 2011). Even at the Paibian stratotype section, the base of the SPICE does not correspond to the base of the *G. reticulatus* zone but to the upper *G. stolidotus* biozone situated below (see Peng *et al.* 2004). At the Siberian Kulyumbe section, the rise in $\delta^{13}C$ seems to start directly at the *G. reticulatus* zone and culminates in a maximum value of *c.* +5 ‰ (Kouchinsky *et al.* 2008; Woods *et al.* 2011). Within the Wanliangyu section (Shandong Province, North China) the proposed SPICE event reaches a peak value of +3.5 ‰ and covers the uppermost *Neodrepanura*, the *Chuangia* and the lowermost *Changshania-Irvingella* trilobite zones (Chen *et al.* 2011). Consequently, the rise of the $\delta^{13}C$ values starts clearly prior to the FAD of *G. reticulatus* of time-equivalent sections (Geyer & Shergold, 2000). The same section is repeatedly published by Chen *et al.* (2012) who shifted the SPICE excursion into a higher stratigraphic position, now starting at the basal *Chuangia* biozone. However, the general problem of sections of the Shandong Province is the missing *Prochuangia* biozone that normally occurs between the *Neodrepanura* and *Chuangia* biozones (Chen *et al.* 2011, 2012). This absence is probably caused by a non-deposition during subaerial exposure (Chen *et al.* 2011). In consequence, a fundamental portion of the $\delta^{13}C$ curve is probably absent, hiding information about its original duration, magnitude and shape. The starting point of the SPICE event at the basal *Chuangia* biozone (as illustrated by Chen *et al.* 2012, fig. 10) therefore has to be wrong. Within the Tangwangzhai section, North China, the peak value of the proposed SPICE event reaches +2.2 ‰ and covers the uppermost *Neodrepanura* to basal *Changshania-Irvingella* trilobite zones (Zhu *et al.* 2004, fig. 4). The *Prochuangia* biozone is again absent, likely explaining the small magnitude of the SPICE at this location. Similar to the Wanliangyu section of Chen *et al.* (2011), the SPICE at Tangwangzhai starts below the *G. reticulatus* biozone. The SPICE excursion of the Shuangqiao section (Hubei Province, North China) starts at the uppermost *Neodrepanura* zone and covers the *Prochuangia* – lower *Changshania-Irvingella* zones (Ng, Yuan & Lin, 2014). A maximum of +3.2 ‰ is reached in the lower *Chuangia* biozone which is followed by a short prominent negative excursion (−1.5 ‰) and a subsequent rise to almost maximum values (Ng, Yuan & Lin, 2014). Again, the $\delta^{13}C$ excursion starts prior to the FAD of *G. reticulatus*.

At the Australian Mount Whelan 1 drillcore $\delta^{13}C_{carb}$ data start to rise clearly prior to the FAD of *G. reticulatus*, reaching a peak value of >6 ‰ in the upper Paibian (upper Idamean according to the Australian nomenclature; Geyer & Shergold, 2000; Kruse, Jago & Laurie, 2009; Gill *et al.* 2011). Biostratigraphy shows that isotope data cover a late Guzhangian – early Jiangshanian (late Mindyallan – early Iverian) interval (Green & Balfe, 1980; Saltzman *et al.* 2000) and not only the Guzhangian–Paibian interval (Gill *et al.* 2011). $\delta^{13}C_{carb}$ data of the Australian Mount Murray section rise from +2.4 ‰ to a peak value of +4.2 ‰ some metres above the FAD of *Irvingella tropica* (Shergold, 1982, 1993) and show a subsequent decrease towards +1.0 ‰ (Gill *et al.* 2011; Fig. 5). Data cover a Paibian–Jiangshanian interval (Idamean–Iverian; Geyer & Shergold, 2000; Kruse, Jago & Laurie, 2009). According to Shergold (1982, 1993), *I. tropica* occurs at 87 m at the Mount Murray section and defines the Iverian base (Geyer & Shergold, 2000). This datum was misused by Gill *et al.* (2011) who plotted *I. tropica* at *c.* 120 m, consequently shifting the Idamean–Iverian boundary into a stratigraphic younger position. However, a correlation with $\delta^{13}C_{carb}$ data of the nearby Mount Whelan 1 drillcore suggests a position of Mount Murray data at the maximum point to decreasing limb of the SPICE (Gill *et al.* 2011). Considering the low sampling density of the Mount Murray section, it is hard to compare the $\delta^{13}C_{carb}$ curves of both sections precisely (Fig. 5). At sections of Missouri (TE-1Texas County Core) and Newfoundland (Felix Cove section), the rise in $\delta^{13}C$ pre-dates the FAD of *Aphelaspis* which is equivalent to the *G. reticulatus* zone (Geyer & Shergold, 2000; Hurtgen, Pruss & Knoll, 2009; Gill *et al.* 2011). At the Laurentian House Range and Lawson Cove sections (both Utah; Saltzman, Runnegar & Lohmann, 1998) documentation begins at the basal *Aphelaspis* zone (equivalent to the *G. reticulatus* zone; Geyer & Shergold, 2000), preventing characterization of the SPICE onset.

It becomes obvious that, despite the general similarities documented for the SPICE in all studied sections, the individual peak values and amplitudes differ (Ahlberg *et al.* 2009; Woods *et al.* 2011). The most-negative $\delta^{13}C_{carb}$ values are recorded from Newfoundland (+1.8 ‰; Hurtgen, Pruss & Knoll, 2009; Fig. 5) whereas the most-positive data are reported from Kazakhstan (+5 ‰, this study; Saltzman *et al.* 2000; Figs 2, 5), South China (+5 ‰; Wa'ergang section; Saltzman *et al.* 2000) and Australia (>6 ‰; Mount Whelan 1 core; Saltzman *et al.* 2000; Gill *et al.* 2011; Fig. 5). For sections of North China, variations in the magnitude of $\delta^{13}C_{carb}$ values are probably related to the absence of the *Prochuangia* biozone. Discrepancies in onset, peak values and shape of the SPICE are generally attributed to biostratigraphic uncertainties, different thicknesses of individual successions and variations in sample density (Saltzman *et al.* 2000; Ahlberg *et al.* 2009; Woods *et al.* 2011). While differences in the magnitude of isotope excursions are probably related to the chemical gradient of seawater, there is no reason for biostratigraphic discrepancies misdating the onset of the SPICE if a well-established palaeontological database supports the geochemical data. According to the rules for biostratigraphic correlation of the International Commission on Stratigraphy (ICS), the base of a stage or series has to be defined by the FAD of cosmopolitan faunal

https://doi.org/10.1017/S0016756815000187 Published online by Cambridge University Press

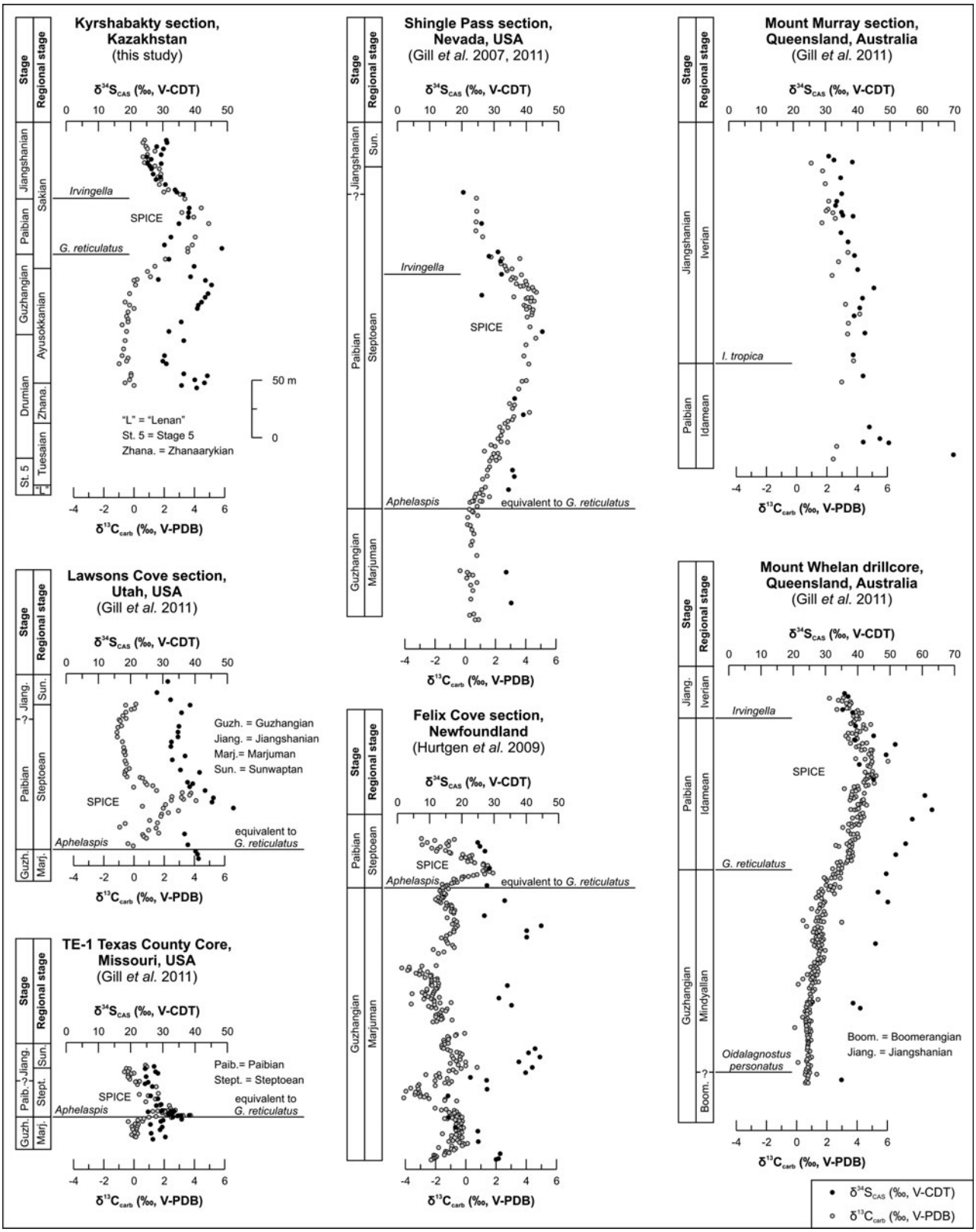

Figure 5. Global comparison of parallel $\delta^{13}C_{carb}$ and $\delta^{34}S_{CAS}$ data during the Cambrian Series 3 to Furongian interval. Data are derived this study, Gill, Lyons & Saltzman (2007), Gill *et al.* (2011) and Hurtgen *et al.* (2009), and are calibrated for uniform vertical and lateral scale. Variations in the onset of local SPICE and SPICE-related $\delta^{34}S_{CAS}$ curves, their peak values, amplitudes and absolute values indicate a heterogeneous Furongian seawater reservoir with respect to sulphate and carbon. Supportive biostratigraphic information is derived from Saltzman *et al.* (1998) for Lawsons Cove and Shingle Pass, from Saltzman *et al.* (2004) and Boyce & Knight (2005) for Felix Cove, from Shergold (1982) for Mount Murray, and from Green and Balfe (1980) and Geyer & Shergold (2000) for Mount Whelan 1.

https://doi.org/10.1017/S0016756815000187 Published online by Cambridge University Press

element. This datum has to be considered as a globally recognizable time-equivalent marker. The FAD of *G. reticulatus* represents such a synchronous stratigraphic datum which defines the base of the Paibian/Furongian (Peng *et al.* 2004; Peng, Babcock & Cooper, 2012). In consequence, variations in the onset of the SPICE should therefore not be an artefact of biostratigraphic discrepancies. However, biostratigraphic information on the onset but also on the duration of the SPICE of some published sections needs re-investigation (e.g. stratigraphic occurrences of *G. reticulatus* and *Irvingella*; see Chen *et al.* 2011, 2012; Gill *et al.* 2011). Frequently, chemostratigraphic studies across the Furongian section lack a detailed (sample to sample basis) biostratigraphic control and in-depth evaluation of the biostratigraphic constraints of the stratigraphic sections under study. This becomes relevant if sample material is limited, as in the case of drillcores. Keeping all these factors in mind, it still seems most probable that differences in $\delta^{13}C$ datasets indicate a Furongian seawater reservoir affected by regional variations. Consequently, the ocean was probably not as homogeneous with respect to $\delta^{13}C$ as generally assumed (see also Hurtgen, Pruss & Knoll, 2009).

6.b. $\delta^{34}S_{CAS}$ and $\delta^{34}S_{CRS}$ values: stratigraphic variations and biostratigraphic constraints

A parallel evolution of carbon and sulphur isotope excursions has been observed from various sedimentary successions of Australia, Sweden and western US (Gill, Lyons & Saltzman, 2007; Gill *et al.* 2011). Our positive excursions in $\delta^{34}S_{CAS}$ and $\delta^{34}S_{CRS}$ occur almost at the same level as the $\delta^{13}C$ excursion, that is, the level of the SPICE (Fig. 2). The $\delta^{34}S_{CRS}$ peak value (31.9 ‰) at Kyrshabakty almost coincides with the carbon isotope maximum. The co-occurrence of these maxima indicates that the amount of organic matter stimulates bacterial sulphate reduction and the formation of pyrite, resulting in the observed ^{34}S enrichment (Gill *et al.* 2011).

Similar to the $\delta^{13}C_{carb}$ values, the onset of excursions, peak values, amplitudes and absolute values of $\delta^{34}S_{CAS}$ and $\delta^{34}S_{CRS}$ vary among the localities (Fig. 5). The most-positive $\delta^{34}S_{CAS}$ values are reported from Mount Murray and Mount Whelan 1 (both Queensland, Australia) with 69.4 ‰ and 62.9 ‰, respectively (Gill *et al.* 2011). The least-positive value (38.1 ‰) is documented from Missouri. At Kyrshabakty the $\delta^{34}S_{CAS}$ peak value of 48.3 ‰ occurs in a stratigraphically lower position than the $\delta^{13}C_{carb}$ maximum (Figs 2, 5). Our $\delta^{34}S_{CAS}$ data increase during the *Lejopyge armata* biozone, culminating in three positive excursions prior to and after the SPICE maximum (Figs 2, 5). This feature is still preserved when considering the least-positive value (28.6 ‰ at K26) as diagenetically altered (Fig. 2). It therefore indicates a stepwise evolution of the SPICE-related positive $\delta^{34}S_{CAS}$ excursion. The large shifts in $\delta^{34}S_{CAS}$ are probably indicative of ocean water which was sensitive to, for example, changes in pyrite burial and/or $\Delta^{34}S$ (Hurtgen, Pruss & Knoll, 2009). Similar pre-SPICE variations could be identified from drillcores of Missouri (TE-1 Texas County Core) and Mount Whelan 1 (Queensland, Australia), and probably from the Felix Cove section of Newfoundland (Fig. 5; Hurtgen, Pruss & Knoll, 2009; Gill *et al.* 2011). Whether the lack of similar trends in $\delta^{34}S_{CAS}$ from sections of Nevada and Utah (Gill, Lyons & Saltzman, 2007; Gill *et al.* 2011) results from limited sampling frequency and/or diagenetic alteration, or reflects the primary isotopic signature of Furongian seawater sulphate sulphur, requires further investigation.

A positive $\delta^{34}S_{CAS}$ excursion prior to the SPICE becomes evident (Fig. 5) when calibrating the various datasets on uniform vertical and horizontal scales. The $\delta^{34}S_{CAS}$ peak pre-dates the SPICE maximum in almost all sections (except Missouri) at different stratigraphic positions (Fig. 5). According to Gill *et al.* (2011), a pre-occurrence of the $\delta^{34}S_{CAS}$ excursion probably indicates a sulphate reservoir which was more sensitive to changes than the marine DIC pool. Differences in stratigraphic position of the onset and the maximum $\delta^{34}S_{CAS}$ values of the SPICE-related $\delta^{34}S_{CAS}$ excursion and variations in their excursion magnitude are indicative of a heterogeneous Furongian seawater sulphate reservoir with low sulphate concentrations (Hurtgen, Pruss & Knoll, 2009; Gill *et al.* 2011). This heterogeneity is not limited to the Upper Cambrian. Comparable differences were also reported by Wotte, Strauss & Sundberg (2011) and Wotte *et al.* (2012) for the traditional Lower–Middle Cambrian boundary interval of Gondwana, Siberia and Laurentia. However, it should be kept in mind that the various datasets of $\delta^{34}S_{CAS}$ and $\delta^{34}S_{CRS}$ were generated using different methods of extraction (Gill, Lyons & Saltzman, 2007; Gill *et al.* 2011; Hurtgen, Pruss & Knoll, 2009; Wotte, Shields-Zhou & Strauss 2012). The consequent and complete elimination of non-CAS sulphur is essential in order to exclude the generation of a mixed $\delta^{34}S_{CAS}$ signal which does not represent the primary composition of seawater. The elimination of non-CAS sulphur often requires consecutive leaching steps (Wotte, Shields-Zhou & Strauss, 2012; Wotte *et al.* 2012). A detailed assessment of prevailing analytical methods revealed that both a consecutive elimination of non-CAS sulphur and a careful evaluation of the degree of diagenetic alteration of the CAS and CRS signals (concentration and isotopic composition) were only rarely realized (Wotte, Shields-Zhou & Strauss, 2012). Caution therefore needs to be applied when comparing/interpreting different datasets of $\delta^{34}S_{CAS}$ and $\delta^{34}S_{CRS}$.

6.c. Evidence for non-euxinic oceanic conditions during the SPICE

The parallel evolution of positive carbon and sulphur isotope excursions during the Furongian has been interpreted as representing widespread ocean anoxia/euxinia and increased burial of pyrite and organic

https://doi.org/10.1017/S0016756815000187 Published online by Cambridge University Press

matter (Gill, Lyons & Saltzman, 2007; Hurtgen, Pruss & Knoll, 2009; Gill *et al.* 2011). Additional evidence for anoxic/euxinic conditions derives from decreasing Mo concentrations during the SPICE event (Gill *et al.* 2011). An increase of anoxia during the SPICE is also indicated by $\Delta^{34}S$ values showing an opposite trend parallel to the positive $\delta^{13}C_{carb}$, $\delta^{34}S_{CAS}$ and $\delta^{34}S_{CRS}$ excursions (Fig. 2). The co-occurrence of low $\Delta^{34}S$ and very positive $\delta^{34}S_{CAS}$ values indicate extensive pyrite burial under euxinic conditions from low and continuously decreasing sulphate concentrations (Gill *et al.* 2011).

However, is the interpretation of widespread subsurface anoxic or even euxinic oceanic conditions really valid for the time interval associated with the SPICE event? The SPICE interval of almost all sections is characterized by the occurrence of benthic faunal elements, clearly indicating the availability of oxygen in the bottom water of worldwide low- to high-latitude environments. Algal mats, brachiopods, sponge spicules, probable conulariids and camaroids, echinoderms and other pelmetazoan ossicles are reported from, for example, the Kyrshabakty section (Kazakhstan; Holmer *et al.* 2001; Koneva & Ushatinskaya, 2010), the Mount Murray section (Queensland, Australia; Shergold, 1982), the Montagne Noire (France; Álvaro *et al.* 2008), Västergötland (Sweden; Ahlberg *et al.* 2005), the Shingle Pass section (Nevada; Palmer, 1965; Saltzman, Runnegar & Lohmann, 1998), the Lawsons Cove section (Utah; R.L. Freeman and J.F. Miller, pers. comm.) and other localities of Arizona, Minnesota, Missouri, Montana, Nevada, Tennessee, Texas, Utah, Wisconsin and Wyoming (e.g. Palmer, 1954; Grant, 1965; Kurtz, 1971, 1975; Freeman & Sitt, 1996; Cowan *et al.* 2005; Rieboldt, 2011; Miller, Evans & Dattilo, 2012). In addition, the SPICE interval of sections of the Port au Port Peninsula (western Newfoundland) is characterized by the occurrence of stromatolites, brachiopods and ostracods (Boyce & Knight, 2005), suggesting a similar fauna for the Felix Cove section (published by Saltzman *et al.* 2004; Hurtgen, Pruss & Knoll, 2009). Proposed widespread euxinic oceanic conditions or even an anoxic event are inconsistent with these data. However, it seems to be most obvious that the deep ocean and sections free of any benthic faunal content reflect regional anoxia (Ahlberg *et al.* 2009).

6.d. Processes forcing the SPICE: cooling phase and/or pH decline

According to Saltzman *et al.* (2000, 2004), the peak of the SPICE corresponds to a maximum regression on Laurentia marked by the continent-wide Sauk II – Sauk III subsequence boundary. Evidence for a drop in sea-level is given for example by a karst surface within the siliciclastic-dominated Davis Formation of Utah, probably coinciding with the Sauk II – Sauk III boundary (Miller *et al.* 2013). Saltzman *et al.* (2000, 2004) discussed a potential linking between globally enhanced weathering of marine carbonate-platform-deposits and a glacial event promoting the SPICE. However, there is no evidence for ice sheets during that interval (Saltzman *et al.* 2000). High $^{87}Sr/^{86}Sr$ values in seawater, probably also induced by widespread sea-level fall, also indicate increased erosion and continental weathering for the SPICE interval (Montañez *et al.* 1996, 2000; Denison *et al.* 1998; Kouchinsky *et al.* 2008). Additional evidence for sea-level fall is given by the exposure of carbonate platforms and the deposition of siliciclastic sequences (e.g. Australia; Lindsay *et al.* 2005) or the collapse of the Aisha-Bibi seamount in the Malyi Karatau Range of Kazakhstan (Cook *et al.* 1991). A drop in sea-level would also contradict the development of widespread euxinic conditions in a variety of marine depositional environments ranging from deeper siliciclastic settings to shelfal carbonate platforms. However, an enhanced continental weathering would also deliver additional sulphate into the seawater, which in turn would be inconsistent with a low seawater sulphate level during the SPICE. This aspect needs further investigation. Indirect indication for a eustatic sea-level fluctuation is given by Elrick *et al.* (2011), who analysed $\delta^{18}O_{phos}$ of phosphatic brachiopods from central and western US. Decreasing $\delta^{18}O_{phos}$ values (from *c.* 15 ‰ to *c.* 13 ‰ V-SMOW) parallel to the rising limb of SPICE would indicate a general warming of seawater during the *Aphelaspis–Dunderbergia* interval (lower Steptoean; Geyer & Shergold, 2000). The proposed warming trend is followed by a successive cooling during the upper *Dunderbergia* and *Elvinia* biozones (upper Steptoean; Geyer & Shergold, 2000). However, such a warming trend is not conformable to a global sea-level fall. Interestingly, our $\delta^{18}O_{carb}$ values show an opposite trend. $\delta^{18}O_{carb}$ data evolve in parallel to $\delta^{13}C_{carb}$, rising from −7.5 ‰ V-PDB (K24) to a maximum of −6.4 ‰ V-PDB (K42), followed by a continuous decrease (Figs 2, 3a). There is no indication that diagenetic processes affected our $\delta^{18}O_{carb}$ data (Figs 3, 4). Furthermore, data fit very well with the known $\delta^{18}O$ record of the entire Cambrian to basal Ordovician section (Jaffrés, Shields & Wallmann, 2007; Prokoph, Shields & Veizer, 2008; Trotter *et al.* 2008). For this reason we consider our $\delta^{18}O_{carb}$ data as representing the primary oxygen isotope signal. Increasing $\delta^{18}O_{carb}$ values during the lower part of the SPICE at the Kyrshabakty section indicate a cooling of seawater, whereas the falling limb would represent a continuous warming trend. This trend in $\delta^{18}O_{carb}$ values is less well developed in Saltzman *et al.* (2000). A similar parallel evolution between $\delta^{13}C_{carb}$ and $\delta^{18}O_{carb}$ is reported from the Siberian Kulyumbe section with peak $\delta^{18}O_{carb}$ values of *c.* −6.0 ‰ and an amplitude of 3–4 ‰ (Kouchinsky *et al.* 2008). In contrast, no sympathetic shifts are documented for paired $\delta^{13}C_{carb}$ and $\delta^{18}O_{carb}$ values available from, for example, the Wa'ergang section (North China; Saltzman *et al.* 2000), the Tangwangzhai section (South China; Zhu *et al.* 2004) or sections in Nevada, Missouri or Tennessee (Glumac & Walker, 1998; Saltzman *et al.* 2000; Gill *et al.* 2011).

https://doi.org/10.1017/S0016756815000187 Published online by Cambridge University Press

Alternatively, the co-varying trend between $\delta^{13}C_{carb}$ and $\delta^{18}O_{carb}$ data could also be interpreted with respect to changes in $[CO_3^{2-}]$ and pH of ocean water. McCrea (1950) and Usdowski & Hoefs (1993) demonstrated that the $\delta^{18}O$ values of rapidly precipitated $CaCO_3$ essentially depend on the pH of the solution. Experiments with living foraminifera have shown that $\delta^{13}C$ and $\delta^{18}O$ of calcite shells become isotopically heavier as seawater pH or $[CO_3^{2-}]$ decrease (Spero *et al.* 1997). This becomes important when applying oxygen isotopes for reconstructing palaeoclimatic or palaeoenvironmental changes (Spero *et al.* 1997; Zeebe, 2001).

Zeebe (1999) demonstrated that an increase of seawater pH by 0.2–0.3 units causes a decrease in $\delta^{18}O$ of 0.22–0.33 ‰, which would usually be interpreted as an increase in seawater temperature. More recently, Uchikawa & Zeebe (2010) calculated the possible effect of the pH on $\delta^{13}C$ and $\delta^{18}O$ during the Paleocene–Eocene thermal maximum (PETM) based on culture experiments with planktonic foraminifera. The authors determined via modelling that a change in pH by −0.1 to −0.3 for the average surface ocean equates to changes in $\delta^{18}O$ and $\delta^{13}C$ of up to 0.7 ‰ and *c.* 2.1 ‰, respectively. Changes in carbon input and release time and/or regional ocean geometry would affect these values accordingly (Uchikawa & Zeebe, 2010). In consequence, a pH decline could probably explain the +1 ‰ shift in our $\delta^{18}O_{carb}$ values during the rising limb of the SPICE. Whether the same correlation between $\delta^{18}O_{carb}$ values and pH could be transferred to inorganically precipitated carbonates needs further investigation (Kim, Hillaire-Marcel & Micci, 2006). Whether a drop in seawater pH could be maintained for a duration of 2–4 Ma (estimated duration of the SPICE; Saltzman *et al.* 2000, 2004) also has to be investigated. If our interpretation is correct, no euxinic conditions would be required to explain the SPICE event. Such a scenario would then be associated with a sea-level rise, as proposed by Peng *et al.* (2004) for the basal Furongian. A transgression probably also resulted in enhanced accumulation of organic matter in shallow-marine shelf environments (Wenger & Baker, 1986) and was therefore associated with fundamental changes in the ocean sulphate and carbonate chemistry, but also in alkalinity.

7. Conclusions

The Furongian base is often associated with the lower part of a eustatic sea-level rise, but also with the onset of a prominent positive excursion in $\delta^{13}C$ (SPICE; Peng *et al.* 2004; Peng, Babcock & Cooper, 2012). In multiple sections, the SPICE co-occurs with positive excursions in $\delta^{34}S_{CAS}$ and $\delta^{34}S_{CRS}$, interpreted as reflecting an elevated rate of organic carbon and pyrite burial during widespread anoxic or euxinic conditions (Gill, Lyons & Saltzman, 2007; Gill *et al.* 2011).

The Furongian Kyrshabakty section, southern Kazakhstan, preserves positive excursions of oxygen isotopes and sulphur isotopes of CAS and CRS in accordance with the positive $\delta^{13}C_{carb}$ peak, identified as the SPICE. The Kazakh SPICE excursion spans an interval ranging from the *Glyptagnostus stolidotus* to the upper *Pseudagnostus vastulus-Irvingella tropica* biozones. Its onset therefore clearly pre-dates the base of the Paibian Stage/Furongian Series identified by the FAD of *Glyptagnostus reticulatus*. A similar positive trend prior to the FAD of *G. reticulatus* is reported for the majority of sections at which the SPICE has been identified (Saltzman *et al.* 2000; Gill, Lyons & Saltzman, 2007; Álvaro *et al.* 2008; Ahlberg *et al.* 2009; Hurtgen, Pruss & Knoll, 2009; Chen *et al.* 2011, 2012; Gill *et al.* 2011; Woods *et al.* 2011). $\delta^{34}S_{CAS}$ data already increase during the *Lejopyge armata* biozone, culminating in three positive excursions prior to and after the SPICE maximum. This three-part evolution indicates a stepwise evolution of the SPICE-related positive $\delta^{34}S_{CAS}$ excursion, characterized by distinct fluctuations. Differences in onset, magnitude and shape of SPICE and SPICE-related $\delta^{34}S_{CAS}$ and $\delta^{34}S_{CRS}$ excursions indicate a Furongian seawater reservoir with low sulphate concentration and heterogeneous in its carbonate carbon and sulphate sulphur isotopic composition.

The SPICE interval of almost all sections offers a diverse benthic fauna, strongly suggesting oxygenated conditions at the seafloor. Proposed widespread euxinic oceanic conditions are inconsistent with these data, but regional anoxia and a euxinic deep ocean cannot be excluded.

Our $\delta^{18}O_{carb}$ values evolve in accordance to the SPICE. The basal rise in $\delta^{18}O_{carb}$ is interpreted as representing a cooling phase, whereas the upper falling limb indicates a continuous warming of seawater. Such climatic variation would be associated with widespread sea-level fall, increased erosion and continental weathering, the exposure of carbonate platforms and the deposition of siliciclastic sequences (Montañez *et al.* 1996, 2000; Denison *et al.* 1998; Saltzman *et al.* 2000, 2004; Lindsay *et al.* 2005; Kouchinsky *et al.* 2008). An alternative interpretation of the parallel $\delta^{13}C_{carb}$ and $\delta^{18}O_{carb}$ trends suggests a close link between seawater pH and $[CO_3^{2-}]$ concentration (McCrea, 1950; Usdowski & Hoefs, 1993; Spero *et al.* 1997; Zeebe, 1999). Modelled changes in pH ranging from −0.1 to −0.3 for the average surface ocean correspond to a +0.7 ‰ and *c.* +2.1 ‰ shift in $\delta^{18}O$ and $\delta^{13}C$, respectively (Uchikawa & Zeebe, 2010). A decline in pH could therefore probably also explain the +1 ‰ shift in our $\delta^{18}O_{carb}$ values.

Data from our recent work challenge much of the interpretations that have been proposed for the SPICE interval. However, the present multitude of uncertainties remaining requires further (re-)investigations of Furongian successions with respect to their isotopes ($\delta^{13}C$, $\delta^{18}O$ and $\delta^{34}S$), elemental concentration and, essentially, their faunal content, allowing a biostratigraphic calibration of sections and strengthening the chemostratigraphic constraints of the SPICE event.

Acknowledgements. We are grateful to Gappar Kh. Ergaliev (Kazakh National Academy of Sciences, Almaty,

https://doi.org/10.1017/S0016756815000187 Published online by Cambridge University Press

Kazakhstan), Michael G. Bassett and Leonid E. Popov (both National Museum of Wales, Cardiff, UK) for organizing the 14th International Conference of the Cambrian Subdivision Working Group in 2009, held in southern Kazakhstan, during which fieldwork and sampling was performed. Anja Cording (University of Cologne), Artur Fugmann and Andreas Lutter (both University of Münster) are thanked for their assistance with isotope analyses. We also thank Dieter Garbe-Schönberg, Ulrike Westernströer and Karin Kissling (all University of Kiel) for performing the ICP-OES analyses. Constructive comments by Benjamin C. Gill (Virginia Tech) greatly improved an earlier version of the manuscript. We thank Alan Jay Kaufman (University of Maryland) and an anonymous reviewer for their helpful comments. Philip Leat (University of Leicester) is thanked for his editorial guidance. Generous funding from the German Research Foundation (Grant WO 1215/4) is gratefully acknowledged.

Declaration of interest

None

References

AHLBERG, P., AXHEIMER, N., BABCOCK, L. E., ERIKSSON, M. E., SCHMITZ, B. & TERFELT, F. 2009. Cambrian high-resolution biostratigraphy and carbon isotope chemostratigraphy in Scania, Sweden: first record of the SPICE and DICE excursions in Scandinavia. *Lethaia* **42**, 2–16.

AHLBERG, P., SZANIAWSKI, H., CLARKSON, E. N. K. & BENGTSON, S. 2005. Phosphatic olenid trilobites and associated fauna from the Upper Cambrian of Västergötland, Sweden. *Acta Palaeontologica Polonica* **50**, 429–40.

ALEXEIEV, D. V., COOK, H. E., BUVTYSHKIN, V. M. & GOLUB, L. Y. 2009. Structural evolution of the Ural–Tian Shan junction: A view from Karatau ridge, South Kazakhstan. *Comptes Rendus Geoscience* **341**, 287–97.

ÁLVARO, J. J., BAULUZ, B., SUBÍAS, I., PIERRE, C. & VINCAÏNO, D. 2008. Carbon chemostratigraphy of the Cambrian-Ordovician transition in a midlatitude mixed platform, Montagne Noire, France. *GSA Bulletin* **120**, 962–75.

BABCOCK, L. E., PENG, S., GEYER, G. & SHERGOLD, J. H. 2005. Changing perspectives on Cambrian chronostratigraphy and progress toward subdivision of the Cambrian System. *Geosciences Journal* **9**, 101–6.

BANNER, J. L. & HANSON, G. N. 1990. Calculation of simultaneous isotopic and trace element variations during water–rock interaction with applications to carbonate diagenesis. *Geochimica et Cosmochimica Acta* **54**, 3123–37.

BOYCE, W. D. & KNIGHT, I. 2005. Cambrian macrofossils from the Phillips Brook and North Brook anticlines, western Newfoundland. Current Research, Newfoundland and Labrador Department of Natural Resources, Geological Survey, Report 05–1, 39–62.

BRAND, U. & VEIZER, J. 1980. Chemical diagenesis of a multicomponent carbonate system. 1: Trace elements. *Journal of Sedimentary Petrology* **50**, 1219–36.

CANFIELD, D. E., RAISWELL, R., WESTRICH, J. T., REAVES, R. C. & BERNER, R. A. 1986. The use of chromium reduction in the analysis of reduced inorganic sulphur in sediments and shales. *Chemical Geology* **54**, 149–55.

CHEN, J., CHOUGH, S. K., HAN, Z. & LEE, J.-H. 2011. An extensive erosion surface of a strongly deformed limestone bed in the Gushan and Chaomidian formations (late Middle Cambrian to Furongian), Shandong Province, China: sequence-stratigraphic implications. *Sedimentary Geology* **233**, 129–49.

CHEN, J., CHOUGH, S. K., LEE, J.-H. & HAN, Z. 2012. Sequence-stratigraphic comparison of the upper Cambrian Series 3 to Furongian succession between the Shandong region, China and the Taebaek area, Korea: high variability of bounding surfaces in an epeiric platform. *Geosciences Journal* **16**, 357–79.

COOK, H. E., TAYLOR, M. E., ZHEMCHUZHNIKOV, S. V., APOLLONOV,, M. K., ERGALIEV, G. K., SARGASKAEV, Z. S. & DUBININA, S. V. 1991. Comparison of two Early Paleozoic carbonate submarine fans: Western United States and southern Kazakhstan, Soviet Union. In *Paleozoic Paleogeography of the Western United States* (eds J. D. Cooper & C. H. Stevens), pp. 847–72. SEPM, Pacific Section 67.

COWAN, C. A., FOX, D. L., RUNKEL, A. C. & SALTZMAN, M. R. 2005. Terrestrial-marine carbon cycle coupling in ~500-m.y.-old phosphatic brachiopods. *Geology* **33**, 661–4.

DENISON, R. E., KOEPNICK, R. B., BURKE, W. H. & HETHERINGTON, E. A. 1998. Construction of the Cambrian and Ordovician seawater $^{87}Sr/^{86}Sr$ curve. *Chemical Geology* **152**, 325–40.

DERRY, L. A. 2010. A burial diagenesis origin of Ediacaran Shuram–Wonoka carbon isotope anomaly. *Earth and Planetary Science Letters* **294**, 152–62.

ELRICK, M., RIEBOLDT, S., SALTZMAN, M. R. & MCKAY, R. M. 2011. Oxygen-isotope trends and seawater temperature changes across the Late Cambrian Steptoean positive carbon-isotope excursion (SPICE event). *Geology* **39**, 987–90.

ERGALIEV, G. K. 1980. Middle and Upper Cambrian trilobites from Malyi Karatau. Alma-Ata: Akademiya Nauk Kazakhskoi SSR, Alma-Ata, 211 pp. (in Russian).

ERGALIEV, G. K. 1981. Upper Cambrian biostratigraphy of the Kyrshabakty section, Malyi Karatau, southern Kazakhstan. In *Short Papers for the Second International Symposium on the Cambrian System* (ed. M. E. Taylor), pp. 82–88. US Geological Survey Open-file Report 81–743.

ERGALIEV, G. K. 1992. On palaeogeography of Karatau (southern Kazakhstan) in Middle Cambrian to Early Ordovician. *Proceedings of Academy of Sciences, Republic of Kazakhstan, Series Geology* **6**, 51–6 (in Russian).

ERGALIEV, G. K. & ERGALIEV, F. G. 2004. Stages and zones of the Middle and Upper portions of Cambrian of Malyi Karatau for the Project of International Stratigraphic Chart. In *Geology of Kazakhstan* (ed. S. Zh. Daukeev), pp. 36–52. Almaty: Kazakhstan Geological Society (in Russian).

ERGALIEV, G. K. & ERGALIEV, F. G. 2008. *Middle and Upper Cambrian Agnostida of the Aksai National Geological Reserve, South Kazakhstan (Kyrshabakty River, Malyi Karatau Range)*. Almaty: Gylym Press, 376 pp. (in Russian with English abstract, introduction and figure captions).

ERGALIEV, G. K., ZHEMCHUZHNIKOV, V. G., ERGALIEV, F. G., BASSETT, M. G., POPOV, L. E. & HOLMER, L. 2009. Field Excursion Guide of the 14th International Field Conference of the Cambrian Stage Subdivision Working Group, International Subcommission on Cambrian Stratigraphy, Malyi Karatau Range, Southern Kazakhstan, 71 pp.

FREEMAN, R. J. & SITT, J. H. 1996. Upper Cambrian and lowest Ordovician articulate brachiopods from the

Arbuckle and Wichita Mountains, Oklahoma. *Journal of Paleontology* **70**, 355–72.

GEYER, G. & SHERGOLD, J. 2000. The quest for internationally recognized divisions of Cambrian time. *Episodes* **23**, 188–95.

GILL, B. C., LYONS, T. W. & FRANK, T. D. 2008. Behavior of carbonate-associated sulfate during meteoric diagenesis and implications for the sulfur isotope paleoproxy. *Geochimica et Cosmochimica Acta* **72**, 4699–711.

GILL, B. C., LYONS, T. W. & SALTZMAN, M. R. 2007. Parallel, high-resolution carbon and sulphur isotope records of the evolving Paleozoic marine sulphur reservoir. *Palaeogeography, Palaeoclimatology, Palaeoecology* **256**, 156–73.

GILL, B. C., LYONS, T. W., YOUNG, S. A., KUMP, L. R., KNOLL, A. H. & SALTZMAN, M. R. 2011. Geochemical evidence for widespread euxinia in the Later Cambrian ocean. *Nature* **469**, 80–3.

GLUMAC, B. & WALKER, K. R. 1998. A Later Cambrian positive carbon-isotope excursion in the southern Appalachians: Relation to biostratigraphy, sequence stratigraphy, environments of deposition, and diagenesis. *Journal of Sedimentary Research* **68**, 1212–22.

GRANT, R. E. 1965. *Faunas and Stratigraphy of the Snowy Range Formation (Upper Cambrian) in Southwestern Montana and Northwestern Wyoming.* Geological Society of America, Memoir no. **96**, 171 pp.

GREEN, P. M. & BALFE, P. E. 1980. Stratigraphic drilling report – GSQ Mt Whelan 1 and 2. *Queensland Government Mining Journal* **81**, 162–78.

HOLMER, L. E., POPOV, L. E., KONEVA, S. P. & BASSETT, M. G. 2001. Cambrian–Early Ordovician brachiopods from Malyi Karatau, the Western Balkhash Region, and Tien Shan, Central Asia. *Special Papers in Palaeontology* **65**, 1–180.

HURTGEN, M. T., HALVERSON, G. P., ARTHUR, M. A. & HOFFMAN, P. F. 2006. Sulfur cycling in the aftermath of a 635-Ma snowball glaciation: evidence for a synglacial sulfidic deep ocean. *Earth and Planetary Science Letters* **245**, 551–70.

HURTGEN, M. T., PRUSS, S. B. & KNOLL, A. H. 2009. Evaluating the relationship between the carbon and sulfur cycles in the later Cambrian ocean: An example from the Port au Port Group, western Newfoundland, Canada. *Earth and Planetary Science Letters* **281**, 288–97.

JACOBSEN, S. B. & KAUFMAN, A. J. 1999. The Sr, C and O isotopic evolution of Neoproterozoic seawater. *Chemical Geology* **161**, 37–57.

JAFFRÉS, J. B. D., SHIELDS, G. A. & WALLMANN, K. 2007. The oxygen isotope evolution of seawater: A critical review of a long-standing controversy and an improved geological water cycle model for the past 3.4 billion years. *Earth-Science Reviews* **83**, 83–122.

KAMPSCHULTE, A., BRUCKSCHEN, P. & STRAUSS, H. 2001. The sulphur isotopic composition of trace sulphates in Carboniferous brachiopods: implications for coeval seawater, correlation with other geochemical cycles and isotope stratigraphy. *Chemical Geology* **175**, 149–73.

KAMPSCHULTE, A. & STRAUSS, H. 2004. The sulphur isotopic evolution of Phanerozoic seawater based on the analysis of structurally substituted sulphate in carbonates. *Chemical Geology* **204**, 255–86.

KAUFMAN, A. J., JACOBSEN, S. B. & KNOLL, A. H. 1993. The Vendian record of C- and Sr-isotopic variations: implications for tectonics and paleoclimate. *Earth and Planetary Science Letters* **120**, 409–30.

KAUFMAN, A. J. & KNOLL, A. H. 1995. Neoproterozoic variations in the C-isotopic composition of seawater: stratigraphic and biogeochemical implications. *Precambrian Research* **73**, 27–49.

KIM, S.-T., HILLAIRE-MARCEL, C. & MICCI, A. 2006. Mechanisms of equilibrium and kinetic oxygen isotope effects in synthetic aragonite at 25 °C. *Geochimica et Cosmochimica Acta* **70**, 5790–801.

KONEVA, S. P. & USHATINSKAYA, G. T. 2010. New brachiopod species from the order Acrotretida from the Cambrian of central Kazakhstan. *Paleontological Journal* **44**, 632–43.

KOUCHINSKY, A., BENGTSON, S., GALLET, Y., KOROVNIKOV, I., PAVLOV, V., RUNNEGAR, B., SHIELDS, G., VEIZER, J., YOUNG, E. & ZIEGLER, K. 2008. The SPICE carbon isotope excursion in Siberia: a combined study of the upper Middle Cambrian–lowermost Ordovician Kulyumbe River section, northwestern Siberian Platform. *Geological Magazine* **145**, 609–22.

KRUSE, P. D., JAGO, J. B. & LAURIE, J. R. 2009. Recent developments in Australian Cambrian biostratigraphy. *Journal of Stratigraphy* **33**, 35–47.

KUMP, L. R. & ARTHUR, M. A. 1999. Interpreting carbon-isotope excursions: carbonates and organic matter. *Chemical Geology* **161**, 181–98.

KUMP, L. R., ARTHUR, M. A., PATZKOWSKY, M. E., GIBBS, M. T., PINKUS, D. S. & SHEEHAN, P. M. 1999. A weathering hypothesis for glaciation at high atmospheric pCO_2 during the Late Ordovician. *Palaeogeography, Palaeoclimatology, Palaeoecology* **152**, 173–87.

KURTZ, V. E. 1971. Upper Cambrian Acrotretidae from Missouri. *Journal of Paleontology* **45**, 53–5.

KURTZ, V. E. 1975. Franconian (Upper Cambrian) trilobite faunas from the Elvins Group of southeast Missouri. *Journal of Paleontology* **49**, 1009–43.

LINDSAY, J. F., KRUSE, P. D., GREEN, O. R., HAWKINS, E., BRASIER, M. D., CARTLIDGE, J. & CORFIELD, R. M. 2005. The Neoproterozoic–Cambrian record in Australia: A stable isotope study. *Precambrian Research* **143**, 113–33.

MARENCO, P. J., CORSETTI, F. A., KAUFMAN, A. J. & BOTTJER, D. J. 2008. Environmental and diagenetic variations in carbonate associated sulfate: an investigation of CAS in the Lower Triassic of the western USA. *Geochimica et Cosmochimica Acta* **72**, 1570–82.

MCCREA, J. M. 1950. On the isotopic chemistry of carbonates and a paleotemperature scale. *The Journal of Chemical Physics* **18**, 849–57.

MILLER, J. F., EVANS, K. R. & DATTILO, B. F. 2012. The great American carbonate bank in the miogeocline of western central Utah: Tectonic influences on sedimentation. In *The Great American Carbonate Bank: The Geology and Economic Resources of the Cambrian–Ordovician Sauk Megasequence of Laurentia* (eds J. R. Derby, R. D. Fritz, S. A. Longacre, W. A. Morgan & C. A. Sternbach), pp. 769–854. AAPG, Memoir no. 98.

MILLER, J. F., EVANS, K. R., KURTZ, V. E. & REPETSKI, J. E. 2013. Biostratigraphy and sequence stratigraphy of Cambrian and lowest Ordovician strata in Missouri. In *Paleozoic Succession in Missouri, Part 1 (revised), Cambrian System* (eds P. S. Mulvany & T. L. Thompson), pp. 13–24. Missouri Geological Survey, Report of Investigations 70.

MONTAÑEZ, I. P., BANNER, J. L., OSLEGER, D. A., BORG, L. E. & BOSSERMAN, P. J. 1996. Integrated Sr isotope variations and sea-level history of Middle to Upper Cambrian platform carbonates: implications for the evolution of Cambrian seawater $^{87}Sr/^{86}Sr$. *Geology* **24**, 917–20.

MONTAÑEZ, I. P., OSLEGER, D. A., BANNER, J. L., MACK, L. E. & MUSGROVE, M. L. 2000. Evolution of the Sr and C

Isotope Composition of Cambrian Oceans. *GSA Today* **10**, 1–7.

NG, T. W., YUAN, J. L. & LIN, J. P. 2014. The North China Steptoean positive carbon isotope excursion and its global correlation with the base of the Paibian Stage (early Furongian Series), Cambrian. *Lethaia* **47**, 153–64.

PALMER, A. R. 1954. The faunas of the Riley Formation in central Texas. *Journal of Paleontology* **28**, 709–86.

PALMER, A. R. 1965. Trilobites of the late Cambrian Pterocephaliid biomere in the Great Basin, United States. US Geological Survey, Professional Paper no. 493, 106 pp.

PALMER, A. R. 1981. Subdivision of the Sauk sequence. In *Short Papers for the 2nd International Symposium on the Cambrian System* (ed. M. E. Taylor), pp. 160–2. United States Geological Survey, Open-File Report 81–743.

PENG, S., BABCOCK, L. E. & COOPER, R. A. 2012. The Cambrian Period. In *The Geological Time Scale 2012*, Volume 2 (eds F. M. Gradstein, J. G. Ogg, M. D. Schmitz & G. M. Ogg), pp. 437–488. Elsevier.

PENG, S., BABCOCK, L. E., ROBISON, R. A., LIN, H., REES, M. N. & SALTZMAN, M. R. 2004. Global standard stratotype-section and point (GSSP) of the Furongian Series and Paibian Stage. *Lethaia* **37**, 365–79.

PENG, S., BABCOCK, L. E., ZUO, J., ZHU, X., LIN, H., YANG, X., QI, Y., BAGNOLI, G. & WANG, L. 2012. Global standard stratotype-section and point (GSSP) for the base of the Jiangshanian Stage (Cambrian: Furongian) at Duibian, Jiangshan, Zhejiang, Southeast China. *Episodes* **35**, 1–16.

PROKOPH, A., SHIELDS, G. A. & VEIZER, J. 2008. Compilation and time-series analysis of a marine carbonate $\delta^{18}O$, $\delta^{13}C$, $^{87}Sr/^{86}Sr$ and $\delta^{34}S$ database through Earth history. *Earth-Science Reviews* **87**, 113–33.

RIEBOLDT, S. 2011. Cambrian inarticulate brachiopods from Nevada and Texas. *Palaeoworld* **13**, 310.

ROWELL, A. J. & BRADY, M. J. 1976. Brachiopods and biomeres. *Brigham Young University Geology Studies* **23**, 165–80.

SALTZMAN, M. R., COWAN, C. A., RUNKEL, A. C., RUNNEGAR, B., STEWART, M. C. & PALMER, A. R. 2004. The Late Cambrian SPICE ($\delta^{13}C$) event and the Sauk II–Sauk III regression: new evidence from Laurentian basins in Utah, Iowa, and Newfoundland. *Journal of Sedimentary Research* **74**, 366–77.

SALTZMAN, M. R., RIPPERDAN, R. L., BRASIER, M. D., LOHMANN, K. C., ROBINSON, R. A., CHANG, W. T., PENG, S., ERGALIEV, E. K. & RUNNEGAR, B. 2000. A global carbon isotope excursion (SPICE) during the Late Cambrian: relation to trilobite extinctions, organic-matter burial and sea level. *Palaeogeography, Palaeoclimatology, Palaeoecology* **162**, 211–23.

SALTZMAN, M. R., RUNNEGAR, B. & LOHMANN, K. C. 1998. Carbon isotope stratigraphy of Upper Cambrian (Steptoean Stage) sequences of the eastern Great Basin: record of a global oceanographic event. *Geological Society of America Bulletin* **110**, 285–97.

SALTZMAN, M. R., YOUNG, S. A., KUMP, L. R., GILL, B. C., LYONS, T. W. & RUNNEGAR, B. 2011. Pulse of atmospheric oxygen during the late Cambrian. *Proceedings of the National Academy of Sciences of the United States of America* **108**, 3876–81.

SHERGOLD, J. H. 1982. Idamean (Late Cambrian) trilobites, Burke River Structural Belt, western Queensland. *Bureau of Mineral Resources, Australia, Bulletin* **187**, 1–69.

SHERGOLD, J. H. 1993. The Iverian, a proposed Late Cambrian Stage, and its subdivision in the Burke River Structural Belt, western Queensland. *BMR Journal of Australian Geology and Geophysics* **13**, 345–58.

SIAL, A. N., PERALTA, S., FERREIRA, V. P., TOSELLI, A. J., ACEÑOLAZA, F. G., PARADA, M. A., GAUCHER, C., ALONSO, R. N. & PIMENTEL, M. M. 2008. Upper Cambrian carbonate sequences of the Argentine Precordillera and the Steptoean C-Isotope positive excursion (SPICE). *Gondwana Research* **13**, 437–52.

SIAL, A. N., PERALTA, S., GAUCHER, C., TOSELLI, A. J., FERREIRA, V. P., FREI, R., PARADA, M. A., PIMENTEL, M. M. & PEREIRA, N. S. 2013. High-resolution stable isotope stratigraphy of the upper Cambrian and Ordovician in the Argentine Precordillera: carbon isotope excursions and correlations. *Gondwana Research* **24**, 330–48.

SPERO, H. J., BIJMA, J., LEA, D. W. & BEMIS, B. E. 1997. Effect of seawater carbonate concentration on foraminiferal carbon and oxygen isotopes. *Nature* **390**, 497–500.

TROTTER, J. A., WILLIAMS, I. S., BARNES, C. R., LÉCUYER, C. & NICOLL, R. S. 2008. Did cooling oceans trigger Ordovician biodiversification? Evidence from conodont thermometry. *Science* **321**, 550–4.

UCHIKAWA, J. & ZEEBE, R. E. 2010. Examining possible effects of seawater pH decline on foraminiferal stable isotopes during the Paleocene-Eocene Thermal Maximum. *Paleoceanography* **25**, PA2216, doi: 10.1029/2009PA001864.

USDOWSKI, E. & HOEFS, J. 1993. Oxygen isotope exchange between carbonatic acid, bicarbonate, carbonate, and water: A re-examination of the data of McCrea (1950) and an expression for the overall partitioning of oxygen isotopes between the carbonate species and water. *Geochimica et Cosmochimica Acta* **57**, 3815–8.

VEIZER, J., ALA, D., AZMY, K., BRUCKSCHEN, P., BUHL, D., BRUHN, F., CARDEN, G. A. F., DIENER, A., EBNETH, S., GODDERIS, Y., JASPER, T., KORTE, C., PAWELLEK, F., PODLAHA, O. G. & STRAUSS, H. 1999. $^{87}Sr/^{86}Sr$, $\delta^{13}C$ and $\delta^{18}O$ evolution of Phanerozoic seawater. *Chemical Geology* **161**, 59–88.

WENGER, L. M. & BAKER, D. R. 1986. Variations in organic geochemistry of anoxic-oxic black shale-carbonate sequences in the Pennsylvanian of the Midcontinent, U.S.A. *Organic Geochemistry* **10**, 85–92.

WOODS, M. A., WILBY, P. R., LENG, M. J., RUSHTON, A. W. A. & WILLIAMS, M. 2011. The Furongian (late Cambrian) Steptoean Positive Carbon Isotope Excursion (SPICE) in Avalonia. *Journal of the Geological Society, London* **168**, 851–61.

WOTTE, T., ÁLVARO, J. J., SHIELDS, G. A., BROWN, B., BRASIER, M. & VEIZER, J. 2007. C-, O- and Sr-isotope stratigraphy across the Lower–Middle Cambrian transition of the Cantabrian zone (Spain) and the Montagne Noire (France), West Gondwana. *Palaeogeography, Palaeoclimatology, Palaeoecology* **256**, 47–70.

WOTTE, T., SHIELDS-ZHOU, G. A. & STRAUSS, H. 2012. Carbonate-associated sulfate: experimental comparisons of common extraction methods and recommendations toward a standard analytical protocol. *Chemical Geology* **326–327**, 132–44.

WOTTE, T., STRAUSS, H., FUGMANN, A. & GARBE-SCHÖNBERG, D. 2012. Paired $\delta^{34}S$ data from carbonate associated sulfate and chromium-reducible sulfur across the traditional Lower–Middle Cambrian boundary of W-Gondwana. *Geochimica et Cosmochimica Acta* **85**, 228–53.

WOTTE, T., STRAUSS, H. & SUNDBERG, F. A. 2011. Carbon and sulfur isotopes from the Cambrian Series

2–Cambrian Series 3 of Laurentia and Siberia. *Museum of Northern Arizona Bulletin* **67**, 43–63.

ZEEBE, R. E. 1999. An explanation of the effect of seawater carbonate concentration on foraminiferal oxygen isotopes. *Geochimica et Cosmochimica Acta* **63**, 2001–7.

ZEEBE, R. E. 2001. Seawater pH and isotopic paleotemperatures of Cretaceous oceans. *Palaeogeography, Palaeoclimatology, Palaeoecology* **170**, 49–51.

ZHU, M., BABCOCK, L. E. & PENG, S. 2006. Advances in Cambrian stratigraphy and paleontology: integrating correlation techniques, paleobiology, taphonomy and paleoenvironmental reconstruction. *Palaeoworld* **15**, 217–22.

ZHU, M., ZHANG, J., LI, G. & YANG, A. 2004. Evolution of C isotopes in the Cambrian of China: implications for Cambrian subdivision and trilobite mass extinctions. *Geobios* **27**, 287–301.

https://doi.org/10.1017/S0016756815000187 Published online by Cambridge University Press